Cell

Article

Sensory circuitry controls cytosolic calcium-mediated phytochrome B phototransduction

Graphical abstract

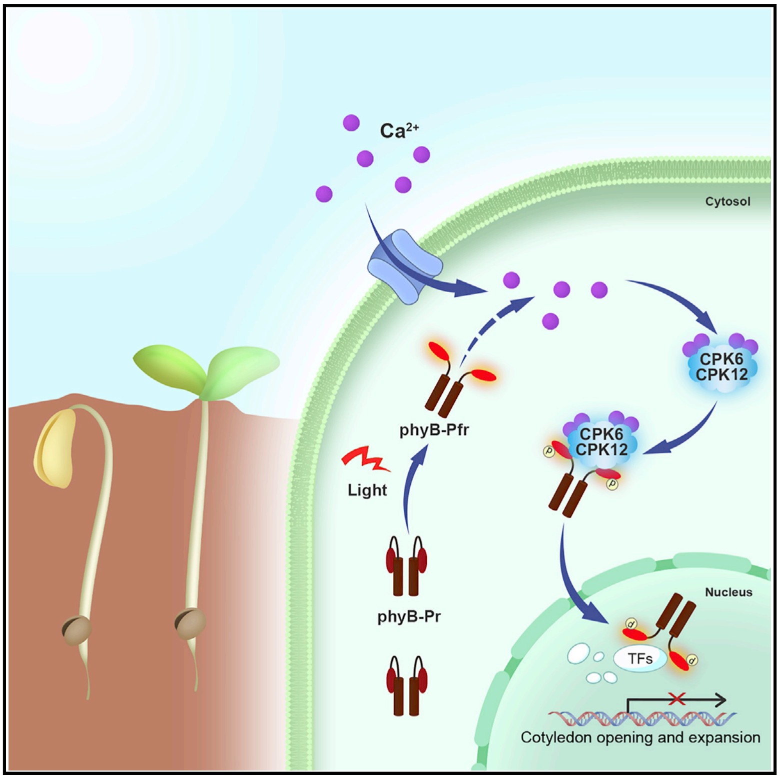

Highlights

- Red light triggers an acute cytosolic Ca^{2+} increase through photoreceptor phyB
- CPK6/12 interact with and phosphorylate phyB depending on both Ca^{2+} and light
- CPK6/12 regulate phyB nuclear import to promote cotyledon opening and expansion
- S80/S106 phosphorylation is required for and generally controls phyB nuclear import

Authors

Yan Zhao, Hui Shi, Ying Pan, ..., Xiaoxia Kou, Xing Wang Deng, Shangwei Zhong

Correspondence

shangwei.zhong@pku.edu.cn

In brief

Red light stimulates an acute cytosolic Ca^{2+} increase to control photoreceptor phyB nuclear translocation, through which it promotes the cotyledon opening and expansion of etiolated *Arabidopsis* seedlings during dark-to-light transition.

Zhao et al., 2023, Cell *186*, 1230–1243
March 16, 2023 © 2023 Elsevier Inc.
https://doi.org/10.1016/j.cell.2023.02.011

CellPress

CellPress

Cell

Article

Sensory circuitry controls cytosolic calcium-mediated phytochrome B phototransduction

Yan Zhao,[1,4] Hui Shi,[2,4] Ying Pan,[1,4] Mohan Lyu,[1] Zhixuan Yang,[1] Xiaoxia Kou,[1] Xing Wang Deng,[1,3] and Shangwei Zhong[1,3,5,*]

[1]State Key Laboratory of Protein and Plant Gene Research, School of Life Sciences, Peking University, Beijing 100871, China

[2]College of Life Sciences, Capital Normal University, and Beijing Key Laboratory of Plant Gene Resources and Biotechnology for Carbon Reduction and Environmental Improvement, Beijing 100048, China

[3]Peking University Institute of Advanced Agricultural Sciences, Shandong Laboratory of Advanced Agriculture Sciences in Weifang, Weifang 261325, China

[4]These authors contributed equally

[5]Lead contact

*Correspondence: shangwei.zhong@pku.edu.cn

https://doi.org/10.1016/j.cell.2023.02.011

SUMMARY

Although Ca^{2+} has long been recognized as an obligatory intermediate in visual transduction, its role in plant phototransduction remains elusive. Here, we report a Ca^{2+} signaling that controls photoreceptor phyB nuclear translocation in etiolated seedlings during dark-to-light transition. Red light stimulates acute cytosolic Ca^{2+} increases via phyB, which are sensed by Ca^{2+}-binding protein kinases, CPK6 and CPK12 (CPK6/12). Upon Ca^{2+} activation, CPK6/12 in turn directly interact with and phosphorylate photo-activated phyB at Ser80/Ser106 to initiate phyB nuclear import. Non-phosphorylatable mutation, phyB$^{S80A/S106A}$, abolishes nuclear translocation and fails to complement *phyB* mutant, which is fully restored by combining phyB$^{S80A/S106A}$ with a nuclear localization signal. We further show that CPK6/12 function specifically in the early phyB-mediated cotyledon expansion, while Ser80/Ser106 phosphorylation generally governs phyB nuclear translocation. Our results uncover a biochemical regulatory loop centered in phyB phototransduction and provide a paradigm for linking ubiquitous Ca^{2+} increases to specific responses in sensory stimulus processing.

INTRODUCTION

Ca^{2+} is the most versatile intracellular second messenger and is ubiquitously involved in numerous stimulus-specific biological processes. How the paradoxical versatility and specificity of Ca^{2+}-mediated signaling are achieved has been a long-standing puzzle.[1–3] In plants, changes in the cytosolic calcium concentration ($[Ca^{2+}]_{cyt}$) have been implicated in the transmission of diverse responses to environmental stresses. For instance, a variety of stimuli, such as soil salinity, touch, drought, extreme temperature, or herbivore attack, evoke an acute, transient $[Ca^{2+}]_{cyt}$ increase, which is sensed and relayed into distinct physiological outputs.[4–10] The fundamental question of how the specificity of a particular signaling pathway is defined by $[Ca^{2+}]_{cyt}$ transients then arises.

Light is a critical environmental factor that exerts a wide range of biological effects. Decades ago, red light has been reported to induce $[Ca^{2+}]_{cyt}$ increases in algae and in protoplasts.[11–13] Early biochemical evidence further shows that microinjecting Ca^{2+} into tomato hypocotyl cells promotes light-responsive gene activation,[14,15] implicating Ca^{2+} in light signaling. Although it has been well established that Ca^{2+} functions as an obligatory intermediate in the cascade of visual transduction and photoreceptor light adaptation in animals,[16] the lack of putative target proteins of Ca^{2+} or any genetic evidence means that the mechanism underlying Ca^{2+} signaling in plant phototransduction remains unidentified.

Plants utilize light as a source of both energy and information cues about their surrounding environment. After geminating in subterranean darkness, plant seedlings undergo etiolated growth. Light triggers a dramatic transition from skotomorphogenic to photomorphogenic development, termed de-etiolation, when plants emerge from the soil.[17,18] The light signals initiating this vital transition are primarily perceived by photoreceptor phytochromes (phys, phyA through phyE in *Arabidopsis*).[19–22] As the dominant red light photoreceptor, phyB is characterized by switching between two photoreversible conformers.[23–27] In dark-grown seedlings, phyB proteins accumulate in the cytoplasm in their biologically inactive red-light-absorbing form (Pr).[23,24,28] Upon light activation, phyB proteins are photoconverted into their biologically active far-red-light-absorbing form (Pfr) and rapidly translocate into the nucleus, where they directly interact with and induce the degradation of transcription factors (TFs) to alter gene expression.[29–34] Thus, the light-dependent nuclear import of photoreceptors is an early determinant step in phy signal transduction that delivers light information from its perception in the cytoplasm directly to nuclear events.

 © 2023 Elsevier Inc.

Here, we show that red light exposure evokes a robust $[Ca^{2+}]_{cyt}$ increase in seconds, which is stimulated by photoreceptor phyB and sensed by two calcium-dependent protein kinases, CPK6 and CPK12 (CPK6/12). We find that CPK6/12 directly interact with and phosphorylate phyB upon activation by Ca^{2+} and light, respectively. Phosphorylation of phyB at S80 and S106 residues generally determines the nuclear translocation of phyB, in which CPK6/12 play a predominant role during initial light exposure of etiolated seedlings. This phyB-Ca^{2+}-CPK6/12-phyB regulatory loop triggers stimulus-specific responses by coordinating cytosolic Ca^{2+} signaling and light information into the phosphorylation and nuclear import of phyB, thus providing insights into the mechanisms of phyB nuclear translocation and the action of calcium in plant light signaling.

RESULTS

Red light triggers a transient $[Ca^{2+}]_{cyt}$ increase through phyB

To investigate the roles of Ca^{2+} in light signaling, we first examined light-induced live $[Ca^{2+}]_{cyt}$ changes by using transgenic aequorin (AEQ) seedlings.[4] When exposing 3-day-old etiolated AEQ seedlings to red light (peaks at approximately 670 nm with a 10-nm half bandwidth), a pronounced increase in $[Ca^{2+}]_{cyt}$ was stimulated within 30 s (Figures 1A and 1B). Either chelating exogenous Ca^{2+} with EGTA or blocking calcium channels with $LaCl_3$ abolished the light-induced $[Ca^{2+}]_{cyt}$ elevation (Figures 1A and 1B). As the control, no measurable luminescence above background was detected in the red-light-irradiated wild-type (WT) seedlings with coelentrazine pretreatment or AEQ seedlings without coelentrazine pretreatment (Figure S1A). These results indicate that red light triggered a Ca^{2+} influx in etiolated seedlings. Because the etiolated seedling has long hypocotyl with closed cotyledons, individual seedling cannot be placed in a fixed position in the solution to count the luminescence accurately using luminometer. We then performed AEQ-based calcium calibration using 9-day-old, dark-adapted seedlings. Time-lapse recording analysis revealed a resting $[Ca^{2+}]_{cyt}$ level of $\sim$108 nM that was transiently elevated to $\sim$221 nM in response to red light, followed by a rapid decrease to basal levels within 2 min (Figure 1C). Neither far-red nor green light evoked significant cytosolic Ca^{2+} changes, and the red-light-triggered increase in $[Ca^{2+}]_{cyt}$ exhibited a red/far-red light reversibility (Figures 1D and 1E), suggesting a specific response of phyB. To further verify whether phyB is required, we generated AEQ/*phyB-9* (AEQ/*phyB*) by genetic cross and examined the $[Ca^{2+}]_{cyt}$ changes in it (Figures 1F and 1G). Comparing with WT background, the red-light-stimulated $[Ca^{2+}]_{cyt}$ increase was mostly abolished in *phyB* mutant (Figures 1F and 1G). These results demonstrate a specific red-light-triggered increase in $[Ca^{2+}]_{cyt}$ through phyB.

Ca^{2+} signaling is required for the light-induced phyB nuclear import

We next wondered whether this light-triggered $[Ca^{2+}]_{cyt}$ transient is physiologically related to light responses. 3-day-old etiolated WT seedlings were transferred into red light exposure for 10 min. RT-qPCR analysis showed that the transcription of light-responsive marker genes, including *PIL1*, *IAA29*, and *HLS1*, was altered (Figure 1H). Notably, inhibiting Ca^{2+} influx by using either $LaCl_3$ or EGTA significantly repressed the light responses of these genes (Figure 1H), indicating that Ca^{2+} influx is involved in light-regulated gene expression.

The cytoplasmic-to-nuclear translocation determines red light signal transducing to photo-responsive genes, yet the regulatory mechanism is unclear.[29,35,36] The involvement of Ca^{2+} influx in light-regulated gene expression prompted us to wonder whether Ca^{2+} mediates the nuclear import of phyB. To test this hypothesis, we assessed the effects of Ca^{2+} on phyB subcellular localization by fluorescence imaging and fractionation immunoblot analysis using *35S:phyB-GFP* (PBG) transgenic plants. Consistent with previous reports,[30] phyB-GFP entered the nucleus upon red light irradiation (Figure 1I). An intriguing observation was that the phyB-GFP signals were rarely detected in the nucleus in either EGTA- or $LaCl_3$-treated samples without affecting total phyB-GFP protein levels (Figures 1I and S1B). Immunoblot analysis further showed that the light-induced nuclear phyB accumulation was largely repressed by EGTA application (Figures 1J and S1C). These findings suggest that the $[Ca^{2+}]_{cyt}$ increase precedes and is necessary for light-induced phyB nuclear translocation.

CPK6 and CPK12 interact with phyB in a light- and calcium-dependent manner

As the main calcium signal decoders, CPKs undergo Ca^{2+}-binding-regulated conformational changes to stimulate their kinase activity and transmit Ca^{2+} signals.[37–39] In search of putative targets potentially involved in specifically relaying light-triggered $[Ca^{2+}]_{cyt}$ transients, CPK6 and CPK12 (CPK6/12) were identified as phyB-interacting proteins. *CPK6* and *CPK12* belong to subgroup I *CPK* gene family[39,40] (Figure 2A). Firefly luciferase complementation imaging (LCI) assays showed that strong luciferase activity was specifically reconstituted when phyB was co-expressed with CPK6 or CPK12 in tobacco leaves (Figure 2B). Although CPK5 and CPK6 show high similarity, their variable and intrinsically disordered N-terminal domains might mediate to form distinct intermolecular interfaces for phyB recognition.[40–43] These results suggest that CPK6 and CPK12 may play specific roles in phyB signaling; nevertheless, what sequence feature or protein topology shared by CPK6 and CPK12 leads to selective interaction with phyB is unknown.

We next explored whether the associations between CPK6/12 and phyB are light regulated. 35S:CPK6/*12-Myc* transgenic plants were used to investigate the interactions of phyB with CPK6/12 in *Arabidopsis* seedlings. Few endogenous phyB proteins were coimmunoprecipitated by CPK6/12-Myc in etiolated seedlings, whereas red light exposure strongly increased the abundance of coimmunoprecipitated phyB proteins (Figures 2C, 2D, S1D, and S1E). Together with semi-*in vivo* immunoprecipitation of phyB-GFP and MBP-CPK6/12 proteins (Figures S1F–S1I), it is indicated that red light enhances the interaction of CPK6/12 and phyB. To assess the physical binding of CPK6/12 and phyB *in vitro*, we performed pull-down assays in which the interactions between MBP-CPK6/12 and His-tagged photo-inactive or active conformers of phyB (phyB-Pr or phyB-Pfr) were examined in the absence or presence of Ca^{2+}. The

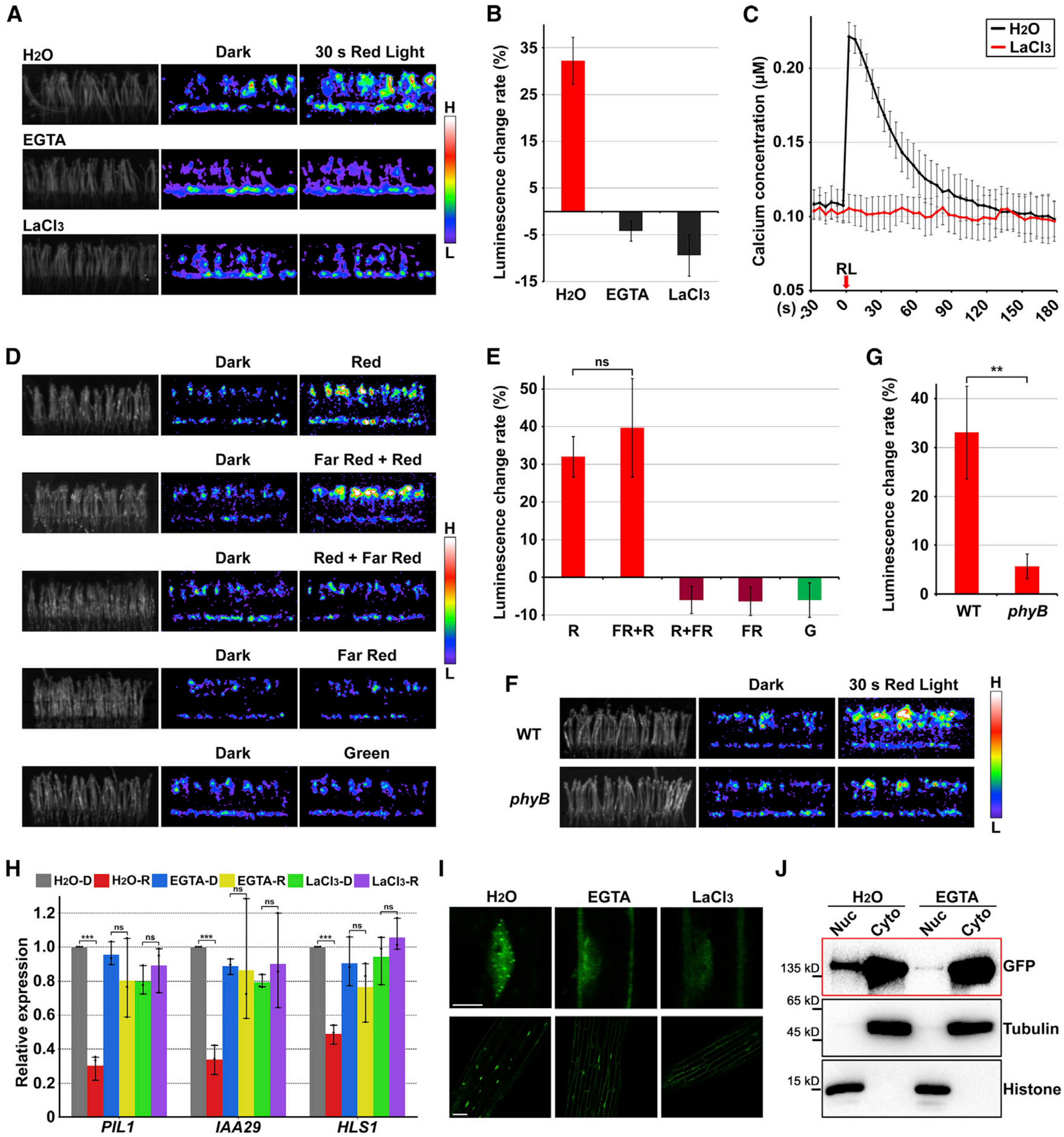

Figure 1. Red-light-triggered cytosolic Ca^{2+} influx through phyB is essential for light-induced phyB nuclear import

(A and B) Representative images (A) and quantification (B) of aequorin bioluminescence indicating that red light triggers Ca^{2+} influx in *Arabidopsis* seedlings. AEQ seedlings pretreated with H_2O, EGTA, or $LaCl_3$ for 10 min were imaged as the dark control and were then irradiated with 30 s of red light, followed by imaging. Luminescence change rate ($\Delta L/L0$) was calculated as: the luminescence intensity of the light-irradiated sample minus that of the dark control sample and then was divided by the luminescence intensity of the dark control sample. Mean ± SD, n = 3.

(C) Time course analysis of red-light-stimulated $[Ca^{2+}]_{cyt}$ elevation. AEQ seedlings were pretreated with either H_2O or 5-mM $LaCl_3$ for 10 min. RL represents 1 min of red light irradiation. Mean ± SD, n = 3.

(D and E) Representative images (D) and quantification (E) of aequorin bioluminescence under different wavelengths of light. AEQ seedlings were imaged as the dark control and were then irradiated with 30 s of the indicated light, followed by imaging. Mean ± SD, n = 3.

(F and G) Representative images (F) and quantification results (G) of aequorin bioluminescence. AEQ (WT) or AEQ/*phyB-9* (*phyB*) seedlings were imaged as the dark control, and the seedlings were then irradiated with 30 s of red light, followed by imaging. Mean ± SD, n = 3.

(H) RT-qPCR results for the early light-responsive gene expression. Etiolated seedlings with H_2O, EGTA, or $LaCl_3$ treatment were either maintained in darkness (D) or irradiated with red light (R) for 10 min. Mean ± SD, n = 3.

(I) Subcellular fluorescence observations of red-light-induced phyB nuclear import. *35S:phyB-GFP* (PBG) etiolated seedlings with H_2O, 5-mM EGTA, or 5-mM $LaCl_3$ treatment were irradiated with red light. Scale bars, 10 μm (top) and 50 μm (bottom).

(J) Representative subcellular immunoblot images of phyB-GFP proteins. PBG etiolated seedlings with H_2O or 5 mM EGTA treatment were irradiated with red light. Nuc, nuclear fractions; Cyto, cytoplasmic fractions.

See also Figure S1 and Methods S1 and S2.

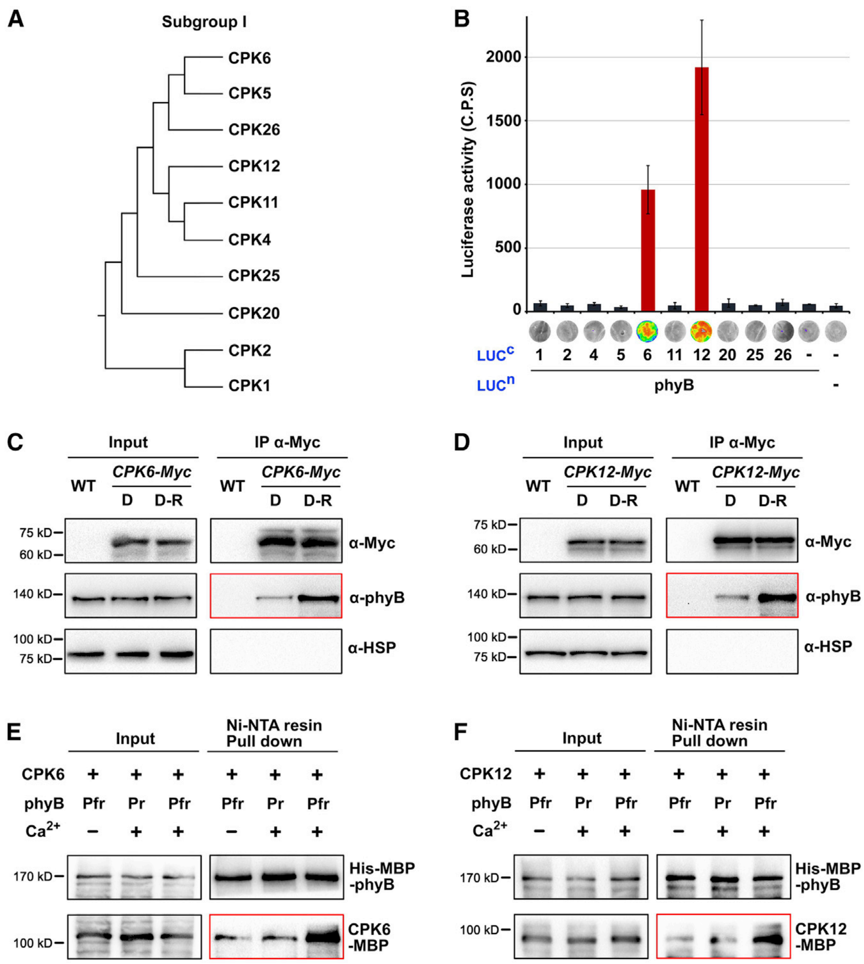

Figure 2. phyB physically interacts with CPK6/12 in a light- and Ca^{2+}-dual-dependent manner

(A) Relationship tree of subgroup I CPKs based on alignment of protein sequences.

(B) LCI assays showing the protein-protein interactions of phyB with individual members of the subgroup I CPKs in tobacco leaves. Full-length phyB or individual CPK was fused in frame with the split luciferase (LUC^n or LUC^c). −, empty vector; C.P.S., counts per second. Mean ± SD, n = 3.

(C and D) CoIP assays showing the associations of phyB and CPK6 (C) or CPK12 (D) in *Arabidopsis* seedlings. Etiolated 35S:CPK6-*Myc* (C) or 35S:CPK12-*Myc* (D) seedlings were either maintained in the dark (D) or irradiated with red light (D to R) for 0.5 h and then were subjected to extraction.

(E and F) CPK6 (E) and CPK12 (F) preferentially interact with the active Pfr conformer of phyB in a Ca^{2+}-dependent manner. Pull-down was performed in the absence (−, 1-mM EGTA) or presence (+, 0.5-mM $CaCl_2$) of Ca^{2+}. Ni-NTA resin was used to pull-down the MBP-CPK6 (E) or MBP-CPK12 (F) bait proteins.

See also Figure S1.

MBP-CPK6/12 proteins preferentially bound to the photo-activated phyB-Pfr in the presence of Ca^{2+} (Figures 2E, 2F, S1J, and S1K). In the parallel controls, very few MBP-CPK6/12 proteins were pulled down by either inactive phyB-Pr in the presence of Ca^{2+} or active phyB-Pfr in the absence of Ca^{2+} (Figures 2E, 2F, S1J, and S1K). These data collectively reveal the dual dependence of light and Ca^{2+} for the interactions of CPK6/12 and phyB.

CPK6 and CPK12 are required for the light-induced nuclear import of phyB

Given that both phyB nuclear translocation and CPK6/12-phyB interaction require the coaction of light and Ca^{2+}, we detected whether CPK6/12 affect phyB nuclear import. Immunoblot analysis showed that endogenous phyB existed exclusively in the cytoplasmic fractions of dark-grown WT seedlings and became detectable in the nuclear fractions after 2 h of red light irradiation (Figures 3A and S2A). External Ca^{2+} application notably accelerated this process (Figures 3A and S2A). However, no phyB proteins were detected in the nuclear fractions of red-light-treated *cpk6 cpk12* mutant, and this defect could not be restored by external Ca^{2+} application (Figures 3A and S2A). The requirement of CPK6/12 for light-induced phyB nuclear translocation was further supported by subcellular fluorescence imaging. Using the CRISPR-Cas9 gene editing technique, we mutated *CPK6* and *CPK12* in the PBG background (PBG/*cpk6 cpk12-Cas*) (Figure S2B). The protein levels of phyB-GFP were not altered (Figure S2C), but red-light-triggered nuclear import of phyB-GFP was greatly reduced in PBG/*cpk6 cpk12-Cas* seedlings (Figure 3B). These results demonstrate that CPK6 and CPK12 mediate the red-light-induced phyB nuclear translocation.

In addition, we examined the nucleo/cytoplasmic partitioning of phyA in etiolated seedlings exposed to red light. Consistent with previous reports,[44–46] red light irradiation induced the import of phyA from the cytoplasmic-to-nuclear fractions (Figure S2D). Interestingly, red-light-induced nuclear import of phyA was also repressed by EGTA treatment (Figure S2D); however, it was not altered in *cpk6 cpk12* mutant (Figure S2E). These results suggest that CPK6/12 play specific roles in red-light-induced phyB nuclear translocation rather than generally control protein nuclear import.

CPK6 and CPK12 mediate the phyB-PIFs signaling pathway

In the nucleus, phyB directly interacts with TFs phytochrome-interacting factors (PIFs), resulting in the rapid degradation of PIFs and subsequent transcriptional changes.[31,32] To assess whether CPK6/12 are necessary for phyB signaling, we examined whether CPK6/12 function in these primary red light responses. *CPK6/12* mutation did not alter the protein levels of PIF1 or PIF3 in dark-grown seedlings but largely abolished the light-triggered

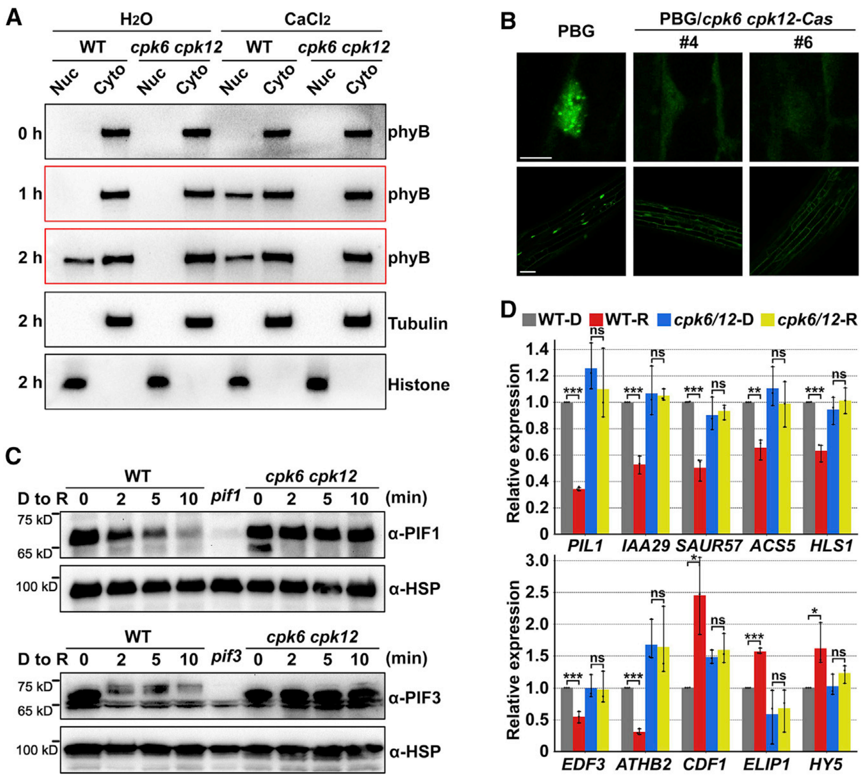

Figure 3. CPK6 and CPK12 are indispensable for red-light-induced nuclear translocation of phyB in light signaling

(A) Subcellular immunoblot analysis indicating that light- and Ca^{2+}-dependent phyB nuclear import is mediated by CPK6 and CPK12. Etiolated seedlings under H_2O or $CaCl_2$ treatment were irradiated with red light for the indicated periods. Nuc, nuclear fractions; Cyto, cytoplasmic fractions.

(B) Subcellular fluorescence observations indicating that CPK6 and CPK12 are required for phyB-GFP nuclear import. Etiolated seedlings were irradiated with red light. Scale bars, 10 μm (top) and 50 μm (bottom).

(C) Immunoblot analysis of PIF1 (top) and PIF3 (bottom) indicating that the red-light-induced degradation of PIF proteins requires CPK6 and CPK12. Etiolated seedlings were irradiated with 10 $\mu mol\ m^{-2}\ s^{-1}$ red light for the indicated periods.

(D) RT-qPCR results showing that CPK6 and CPK12 mediate the light-regulated transcription of PIF direct target genes in the dark-to-light transition. Etiolated WT and *cpk6 cpk12* (*cpk6/12*) seedlings were either maintained in darkness (D) or irradiated with red light (R) for 10 min. Mean ± SD, n = 3.

See also Figure S2.

degradation of PIF1 or PIF3 during the dark-to-light transition (Figures 3C, S2F, and S2G). Moreover, red-light-regulated transcription of PIF direct target genes,[18,47–49] was mostly unchanged in the *cpk6 cpk12* mutant (Figure 3D). These analyses support the essential roles of CPK6/12 in mediating phyB signal transduction.

CPK6 and CPK12 phosphorylate phyB at S80/S106 depending on both light and calcium

Previous studies have shown that a region from 80 to 120 amino acids in the N-terminal extension of phyB is preferentially phosphorylated under light.[50,51] In terms of the serine/threonine protein kinase activity of CPKs, we postulated that phyB might be a substrate of CPK6/12. *In vitro* kinase assays showed that CPK6/12 directly phosphorylated the Pfr phyB N terminus (phyBN, 1–610 amino acids) in the presence of Ca^{2+}, and either the Pr conformer or the absence of Ca^{2+} greatly decreased the phosphorylation of phyBN (Figures 4A, 4B, S3A, and S3B), consisting with the light- and Ca^{2+}-dependent CPK6/12-phyB interactions.

To map the candidate phosphorylation sites of phyB during the dark-to-light transition, phyB-GFP proteins were purified from the dark-grown PBG seedlings without or with 0.5 h of red light exposure and were subjected to mass spectrometry analyses. Three serine residues, S80, S86, and S106, were shown to be phosphorylated with a PTM site probability greater than 99% using phosphoRS algorithm in all replicates (Figures S3C–S3E), and the relative abundance of phosphorylation for S80 and S106 was significantly elevated by red light (Figure 4C). Among these residues, $phyB^{S86A}$ has been reported to exhibit elevated nuclear accumulation under dim red light and show no significant differences from phyB-WT under saturated red light conditions,[52] differing from what was observed in the *cpk6 cpk12* mutant (Figures 3A and 3B). We then assessed the involvement of S80 and S106 in the CPK6/12-mediated phyB phosphorylation. S80 and S106 were mutated to non-phosphorylatable alanine residues (phyBN-2A). Compared with phyBN-WT, phosphorylation of phyBN-2A by CPK6 or CPK12 was largely reduced (Figures 4A, 4B, S3A, and S3B), indicating that S80 and S106 are the target sites responsible for CPK6/12-mediated phyB phosphorylation.

S80/S106 phosphorylation is indispensable for light-induced phyB nuclear import

To investigate whether S80/S106 phosphorylation is involved in light-induced phyB nuclear translocation, different variants of YFP-fused phyB proteins, including WT (phyB-WT), non-phosphorylatable double S80 and S106 mutant (serine to alanine, phyB-2A), and phosphomimic double S80 and S106 mutant (serine to aspartate, phyB-2D), were expressed in *phyB-9* mutant (*phyB-WT*, *phyB-2A*, and *phyB-2D*). Fluorescence imaging observations showed that phyB-WT, phyB-2A, and phyB-2D proteins were located in the cytoplasm of etiolated seedlings (Figure 4D). Upon red light exposure, phyB-WT and phyB-2D proteins were predominantly distributed in the nucleus (Figure 4D). In contrast, the phyB-2A protein was conspicuously retained in the cytoplasm, with no obvious fluorescence signals detected in the nucleus (Figure 4D). Immunoblot analysis further showed that phyB-WT and phyB-2D exhibited light-induced

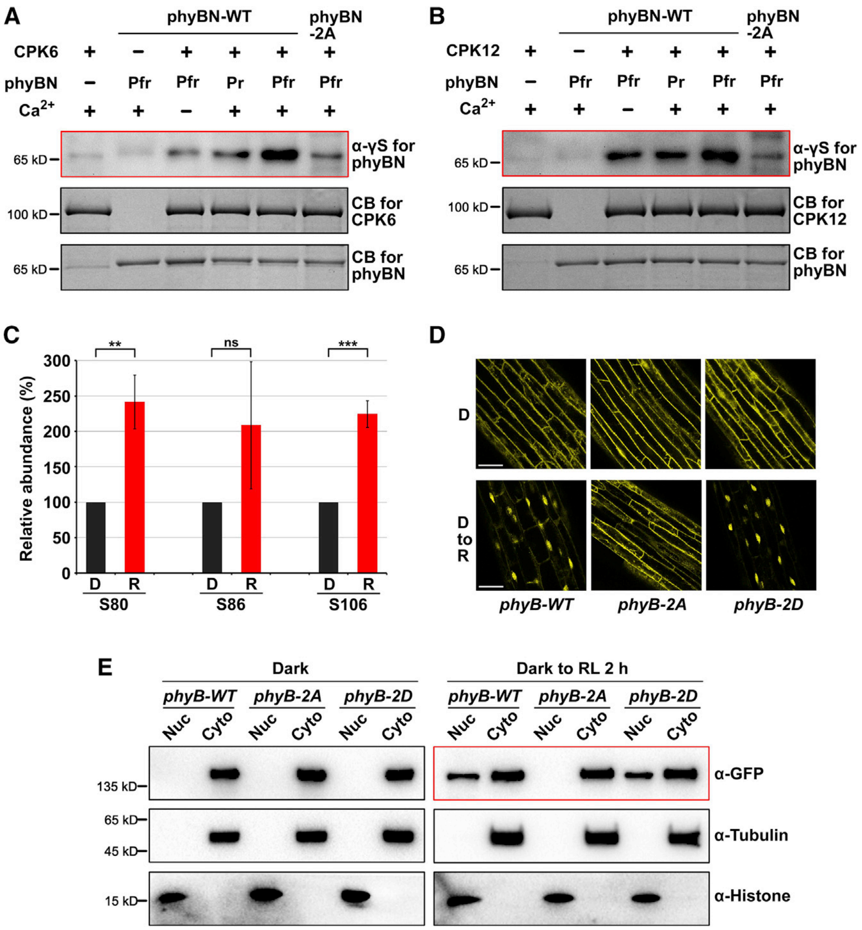

Figure 4. Phosphorylation of phyB at S80/S106 by CPK6/12 drives phyB nuclear translocation

(A and B) *In vitro* kinase assays showing the Ca^{2+}- and light-dependent phosphorylation of phyB at S80/S106 by CPK6 (A) and CPK12 (B). The assays were performed in the absence (−, 1-mM EGTA) or presence (+, 0.5-mM $CaCl_2$) of Ca^{2+}. CB, Coomassie brilliant blue staining.

(C) Relative abundance of phosphorylation at S80, S86, and S106 of phyB during dark-to-light transition. PBG etiolated seedlings were irradiated without (D) or with (R) 0.5-h red light exposure. The precursor abundance ratio at a given site was calculated as the abundance of phosphorylated residues divided by the total abundance of phosphorylated and non-phosphorylated residues. The relative abundance of R sample was expressed relative to that of D sample (set as 100%). Mean ± SD, n = 3.

(D) Subcellular fluorescence observations of phyB-YFP protein in *Arabidopsis* seedlings indicating that the phosphorylation of phyB at S80/S106 contributes to light-induced phyB nuclear import. Etiolated seedlings were maintained in darkness (D) or irradiated with red light (D to R). 2A, S80A and S106A. 2D, S80D and S106D. Scale bars, 50 μm.

(E) Subcellular immunoblot analysis indicating that S80/S106 phosphosites are critical for red-light-induced phyB nuclear translocation. Etiolated seedlings were maintained in darkness (dark) or irradiated with red light (dark to RL 2 h). Nuc, nuclear fractions; Cyto, cytoplasmic fractions.

See also Figures S3 and S4.

nuclear accumulation, while phyB-2A was exclusively located in the cytoplasm, even after 2 h of red light irradiation (Figures 4E and S4A). Considering the results together, we conclude that S80 and S106 are the target sites whereby CPK6/12 mediate light-induced phyB nuclear translocation.

CPK6/12-regulated phyB nuclear import is essential for de-etiolation transition

We next assessed the physiological function of CPK6/12-regulated phyB nuclear translocation. The initial light-induced photomorphogenic transition was defective in *cpk6* and *cpk12* mutants, exhibiting retarded cotyledon opening and expanding phenotype (Figures 5A and 5B). More severe defects of cotyledon were observed in *cpk6 cpk12* double mutant, indicating the functional redundancy of CPK6 and CPK12 (Figures 5A and 5B). The defective cotyledon phenotypes of *cpk6 cpk12* were reminiscent of those observed in *phyB-9* mutant, and *phyB-9 cpk6 cpk12* triple mutant behaved similarly to *phyB-9*, suggesting that CPK6/12 function in phyB signaling pathway for accomplishing de-etiolation transition (Figures 5A and 5B). To verify whether the defective cotyledon phenotypes of *cpk6 cpk12* are due to the impaired phyB nuclear import, we transformed a nuclear localization signal (NLS) fused *phyB-YFP* into *cpk6 cpk12-Cas* mutant (Figure S4B). The NLS-fused phyB-YFP proteins were constitutively localized in the nucleus and photobodies were induced by red light (Figure S4C). With complementing the nuclear localized phyB, the photomorphogenic defects of *cpk6 cpk12-Cas* mutant were fully restored (Figures S4D and S4E). These data demonstrate that CPK6/12 regulate de-etiolation transition through controlling phyB nuclear translocation.

CPK6/12 function specifically in etiolated seedlings upon initial light exposure

Upon prolonged light exposure, the cotyledon defects of *cpk6 cpk12* mutant were gradually relieved from those reminiscent of *phyB*-9 mutant to those of WT (Figures S4F–S4H). Consistently, phyB-GFP nuclear import was largely impaired in *cpk6 cpk12* mutant after 2-h red light exposure but translocated to the nucleus with prolonged irradiation, despite the appearance of small foci with dispersed signals as compared with the large photobodies in WT (Figure S5A). We also examined the hypocotyl elongation of seedlings grown under different day-night conditions or continuous light with various fluence rates, and the results showed that *cpk6 cpk12* mutant exhibits no significant difference from

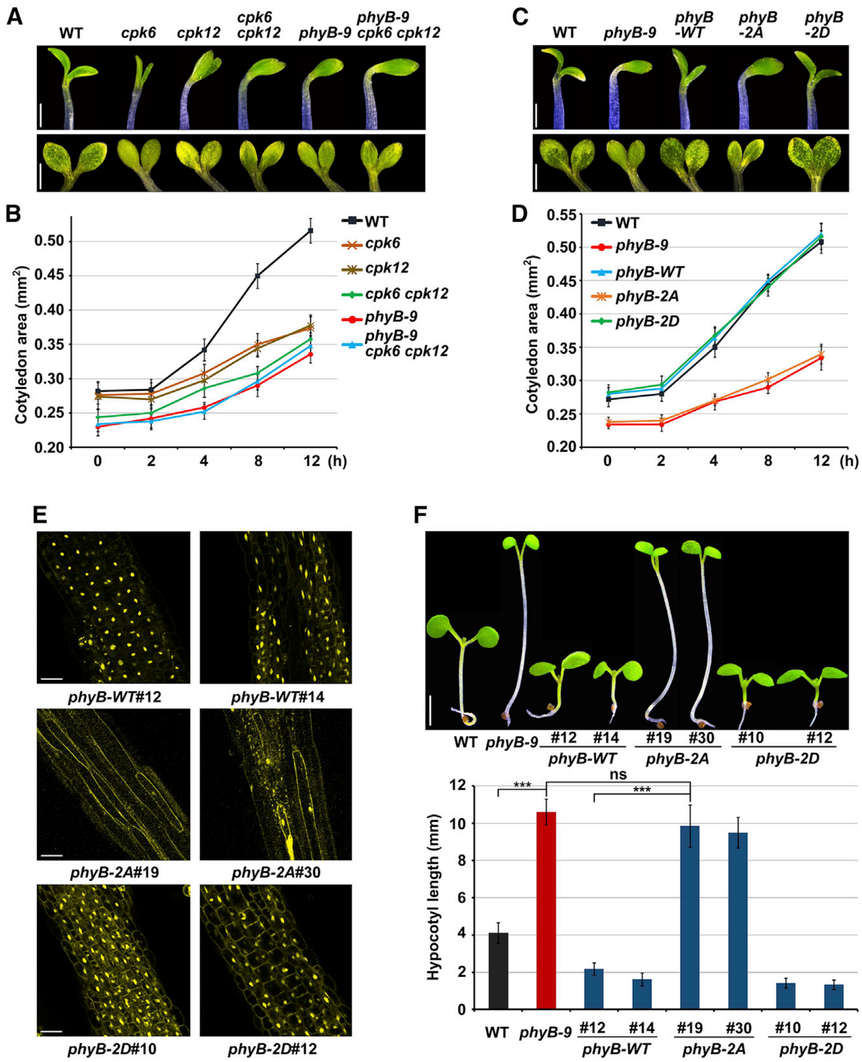

Figure 5. Phosphorylation of phyB at S80/S106 by CPK6/12 mediates phyB's physiological function

(A–D) Representative cotyledon opening (A and C, top) and expanding phenotypes (A and C, bottom) of etiolated seedlings subjected to 10-μmol m^{-2} s^{-1} red-light irradiation for 12 h were shown. Scale bar, 0.5 mm. The cotyledon areas in a red light irradiation time course experiment were quantified (B and D). Mean ± SD, n ≥ 10.

(E) Subcellular fluorescence observations of phyB-YFP proteins in 5-day-old red-light-grown seedlings indicating that the phosphorylation of phyB at S80/S106 is required for the nuclear localization of phyB under continuous red light exposure. Scale bars, 50 μm.

(F) *phyB-WT* and *phyB-2D* but not *phyB-2A* complement the defects of *phyB-9* mutant under continuous red light exposure. Representative images (top) and hypocotyl lengths (bottom) of 5-day-old, red-light-grown seedlings were shown. Scale bars, 2 mm. Mean ± SD, n ≥ 10.

See also Figures S4, S5, and S6.

WT (Figures S5B and S5C). During day-night cycles, phyB-GFP proteins exhibited large-sized photobodies in the day, which dispersed at night, but their nuclear localization remained almost unchanged (Figure S5D),[53,54] indicating that nucleo-cytoplasmic partitioning is not the main regulatory mechanism of phyB under day-night conditions. To investigate whether CPK6/12-mediated phyB nuclear import is tissue or organspecific, we examined phyB nuclear translocation separately in cotyledon and hypocotyl cells, and similar defects were observed in both cotyledon and hypocotyl of *cpk6 cpk12* mutant (Figure S5A). Additionally, CPK6/12 were not obviously altered at either the transcript or protein level during dark-to-light transition, except for a slight decrease in CPK6 protein accumulation after 8 h light irradiation (Figures S5E and S5F). Taken together, we demonstrate that CPK6/12 regulate the nuclear translocation of phyB to promote cotyledon opening and expansion specifically in etiolated seedlings upon initial light exposure.

S80/S106 phosphorylation contributes to phyB signaling outcomes

Next, we analyzed the photomorphogenic phenotypes of *phyB-WT*, *phyB-2A*, and *phyB-2D* transgenic plants. In agreement with the nucleo-cytoplasmic partitioning results, *phyB-2A* exhibited delayed opening and less expanded cotyledons, whereas *phyB-2D* effectively restored the photomorphogenic defects of *phyB-9* mutant (Figures 5C and 5D). During the generation of *phyB-2A* transgenic plants, we noticed that *phyB-2A* always displayed phenotypes similar to those of *phyB-9*. To verify this observation, we further examined the subcellular localization of phyB variants under continuous red light conditions. phyB-WT and phyB-2D proteins predominantly accumulated in the nucleus, while phyB-2A did not undergo nuclear localization, mainly located in the cytoplasm with dim fluorescence observed in the nucleus (Figure 5E). Consistent with the subcellular localization, overexpressing *phyB-2D* restored the defects of *phyB-9* mutant (Figures 5F and S6A). Neither moderate nor high levels of phyB-2A were able to complement *phyB-9* mutant, and these seedlings displayed an etiolated-like long hypocotyl (Figures 5F and S6A). We also observed that *phyB-2D* with higher levels of phyB protein exhibited similar phenotypes as *phyB-WT* (Figures 5D, 5F, and S6A), suggesting that phyB-2D may not be fully functional as phyB-WT. These results are consistent with the reported data showing a partially functional phyB^{S106D}.[50] Collectively, these data indicate the essential roles of phyB phosphorylation at S80/S106 in the nuclear translocation and physiological function of phyB.

S80/S106 phosphorylation controls phyB nuclear import without affecting its activity

Given the essential roles of S80/S106 phosphorylation in phyB function, we assessed whether phyB-2A controls only the nuclear translocation or also affects the biological activity of phyB. CoIP results showed that phyB-2A underwent the light-dependent interactions with PIF1 or PIF3 (Figures 6A and S6B), indicating a normal photo-activation capacity of phyB-2A. We further introduced the *NLS*-fused *phyB-WT*, *phyB-2A*, or *phyB-2D* into *phyB-9* mutant, and transgenic lines with comparable phyB protein levels were chosen (Figure S6C). NLS-fused phyB-WT, phyB-2A, and phyB-2D proteins dispersed evenly in the nucleus of etiolated seedlings and formed speckles either upon 2-h red-light irradiation or under continuous red light (Figures 6B and S6D). Unlike *phyB-2A*, *phyB-2A-NLS* fully restored the photomorphogenic defects of *phyB-9* mutant as *phyB-WT* (Figure 6C). The fluence rate response curves for hypocotyl lengths of *phyB-WT-NLS*, *phyB-2A-NLS*, and *phyB-2D-NLS* seedlings were also similar (Figure S6E). Moreover, adult *phyB-2A* plants still resembled those of *phyB-9* mutant, while *phyB-2A-NLS* complemented the pale-green and long leaf petiole phenotypes of *phyB-9* to restore that of WT (Figures 6D and 6E). These findings demonstrate the full activity of phyB-2A-NLS, supporting the notion that S80/S106 phosphorylation solely controls phyB nuclear translocation.

The phosphorylation-controlled nuclear import mechanism is conserved in phyB, phyD, and phyE

Previous phylogenetic analysis indicated that phyA/C and phyB/D/E diverged more than 300 mya and that S106 was subject to positive selection along with the separation of phys.[55] Alignment of the five *Arabidopsis* phytochrome protein sequences showed that S80/S106 are conserved in phyB/D/E but not in phyA/C (Figure S6F). As noted above, we found that the defects in red-light-regulated rapid gene expression, and PIF1/3 protein degradation were more severe in *cpk6 cpk12* mutant than those in *phyB* mutant (Figures 3C, 3D, S2F, and S2G),[56,57] which cannot be explained by altered nuclear import of phyB alone. We also found that CPK6/12 did not affect the nuclear import of phyA (Figure S2E). These results prompted us to wonder whether CPK6/12-directed phosphorylation also regulates the nuclear translocation of phyD/E. To test this hypothesis, we first detected the protein interactions between CPK6/12 and phyD/E. The LCI results showed that both phyD and phyE interacted with CPK6/12 in tobacco leaves (Figures S7A and S7B). CoIP results further revealed the preferential interactions between CPK6/12 and the Pfr conformer rather than the Pr conformer of phyD/E (Figures S7C and S7D).

To evaluate whether phosphorylation of phyD at S82/S108 or phyE at S44/S68, which are homologous to the S80/S106 of phyB, respectively, contributes to their nuclear translocation, we generated non-phosphorylatable double-mutant phyD-2A and phyE-2A. YFP-fused variants of phyD/E were expressed in tobacco leaves, and the subcellular localization was observed by confocal imaging. We found that phyD-WT and phyD-2A were mainly localized in the cytoplasm of the dark-adapted tobacco epidermal cells (Figure S7E). With red-light irradiation, phyD-WT proteins translocated into the nucleus and formed photobodies. By contrast, phyD-2A proteins retained in the cytoplasm, whereas NLS fusion resulted in the constitutive nuclear localization and light-induced photobody formation of phyD-2A (Figure S7E). On the other hand, phyE underwent light-induced nuclear translocation with less and smaller photobodies, and phyE-2A partially impaired the nuclear import of phyE (Figure S7F). These results reveal that CPK6/12-directed phytochrome phosphorylation for nuclear translocation could be conserved in the phyB/D/E linage. It should be noted that phyA plays a strong role in red-light-induced PIF degradation; thus, the stable PIF proteins in *cpk6 cpk12* mutant may not be fully explained by the defects of phyB/D/E nuclear import. Taken together, S80/S106-controlled nuclear import might contribute to the specificity of phyA- and phyB-branched signaling, suggesting an important role of nucleo-cytoplasmic partitioning in determining the properties of individual photoreceptor members.

DISCUSSION

The discovery of light-dependent phyB nuclear translocation is a milestone in plant photobiology. Numerous attempts had previously been made to determine the cytoplasmic intermediates and cascades participating in the early transduction process.[13–15,23,58,59] With the identification of phyB nuclear localization,[29,44] investigations of phyB signaling shifted to focus on the actions of phyB-PIFs in the nucleus.[17,31,60–63] However, the mechanism by which light signals are transduced to initiate the nuclear import of phyB remains elusive. In this study, we uncover a general mechanism for phyB nuclear translocation controlled by phyB phosphorylation at S80/S106, in which a Ca^{2+}-CPK6/12 pathway is specifically activated and functions during the dramatic developmental transition of etiolated seedlings (Figure 7). Red light triggers an acute increase in $[Ca^{2+}]_{cyt}$ via phyB, causing the activation of two Ca^{2+} sensors, CPK6 and CPK12. In turn, activated CPK6/12 directly interact with and phosphorylate phyB, and additional specificity is achieved by preferential interaction with phyB in the Pfr conformer. CPK6/12 and phyB proteins sense Ca^{2+} and light signals, respectively, followed by the formation of a CPK6/12-phyB module that converts the signals to induce the phosphorylation and nuclear import of phyB-Pfr and, thus, initiate light responses. Hence, our studies shed light on the central role of Ca^{2+} signaling in plant phototransduction and provide the associated molecular framework.

The timely de-etiolation transition is critical for the survival of emergent seedlings. In subterranean darkness, phyB proteins exclusively accumulate in large abundance as the Pr conformer in the cytoplasm. When emerging to reach light, massive photo-activated phyB proteins must enter the nucleus to initiate de-etiolation. The Ca^{2+}-CPK6/12 pathway provides a route for the nuclear import of massive cytosolic phyB in a short time. Seeds can also germinate in the light and then grow under continuous light or day-night conditions. In continuous light, as the newly synthesized phyB is photo-activated and enters the nucleus, there may not be sufficient phyB accumulated in the cytoplasm to stimulate a robust increase in $[Ca^{2+}]_{cyt}$ over the threshold needed to activate CPK6/12. The constitutively active Y276H mutant simulates seedlings grown in light.[64] In day-night

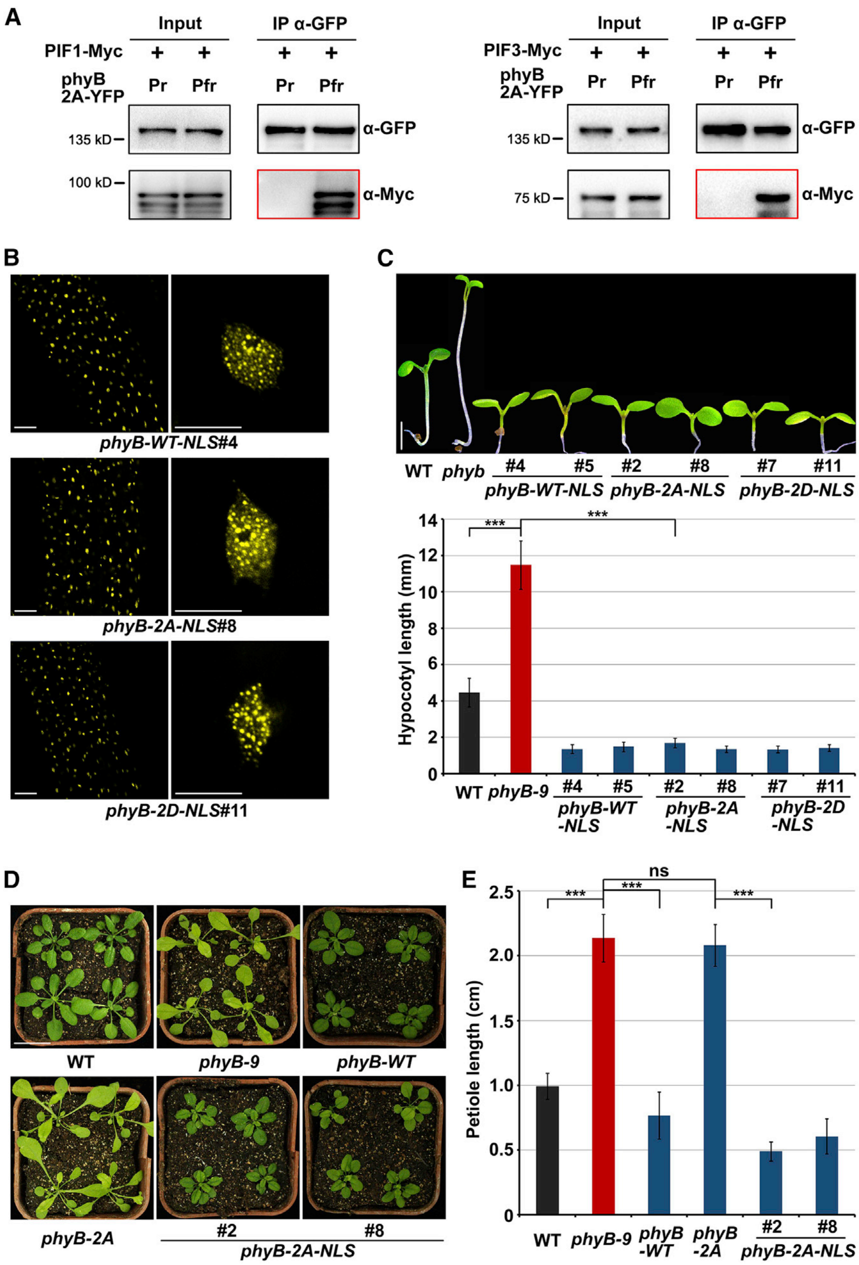

Figure 6. Phosphorylation at S80/S106 is required for the nuclear import but not the activity of phyB

(A) The light-dependent interactions between phyB and PIF1 (left) or PIF3 (right) are not affected by the non-phosphorylatable mutation of S80/S106 in phyB.

(B) Subcellular fluorescence observations of NLS-fused variants of phyB-YFP proteins in 5-day-old red-light-grown seedlings. Scale bars, 50 μm (left) and 10 μm (right).

(C) *phyB-2A-NLS* complements the seedling phenotypes of *phyB-9* mutant. Representative images (top) and hypocotyl lengths (bottom) of 5-day-old, red-light-grown seedlings were shown. Scale bars, 2 mm. Mean ± SD, $n \geq 10$.

(D and E) *phyB-2A-NLS* complements the adult plant phenotypes of *phyB-9* mutant. Representative images (D) and petiole lengths (E) of 4-week, long-day-grown adult plants were shown. Scale bars, 2 cm. Mean ± SD, $n \geq 10$.

See also Figure S6.

conditions, phyB Pfr conformer undergoes thermal reversion during the night; however, it is still retained in the nucleus. Although the newly synthesized phyB may activate Ca^{2+}-CPK6/12 at dawn, since there exists abundant phyB in the nucleus, the physiological outcomes of CPK6/12 could be masked. Thus, S80/S106 phosphorylation imposes a general role, while CPK6/12 specifically function in etiolated seedlings upon initial light exposure in controlling phyB nuclear import. Although we have not found all the kinases responsible for S80/106 phosphorylation, we do show some interesting trends that kinases other than CPK6/12 contribute to the different phenotypes of *cpk6 cpk12* and *phyB-2A* during prolonged light exposure or when seeds germinate in the light. Studies in animals have demonstrated that distinct kinases phosphorylate the same residues of tumor suppressor P53 to regulate cell apoptosis in response to different stimuli.[65,66] As the main photoreceptor, phyB regulates numerous responses throughout the entire life cycle of plants. Various kinases may be adopted to regulate phyB nuclear import during different developmental stages or in response to fluctuating environments.

The nuclear import of phyB is an indispensable and rate-limiting step in phyB signaling.[34,67] We reveal that S80/S106 phosphorylation determines phyB nuclear translocation without altering its activity. Two NLS-bearing proteins, far-red-elongated hypocotyl 1 (FHY1) and FHY1-like (FHL), function as shuttle proteins for phyA nuclear import without changing phyA activity.[36,68–71] It is plausible to hypothesize the existence of NLS-bearing proteins that might recognize the S80/S106 sites phosphorylated phyB-Pfr and transport it into the nucleus. Also, the relationship between phyB phosphorylation and unmasking of NLS-like motif in the C terminus of phyB-Pfr needs investigation.[72] Moreover, mutation of *CPK6/12* mostly abolishes the initial nuclear import of phyB but not phyA; however, EGTA impairs the nuclear import of both phyA and phyB. Since the pharmacological effect of EGTA may be more general, whether EGTA regulates phyA nuclear import via the known FHY1/FHL pathway and how EGTA affects the nuclear import of different phytochromes are important subjects for further studies.

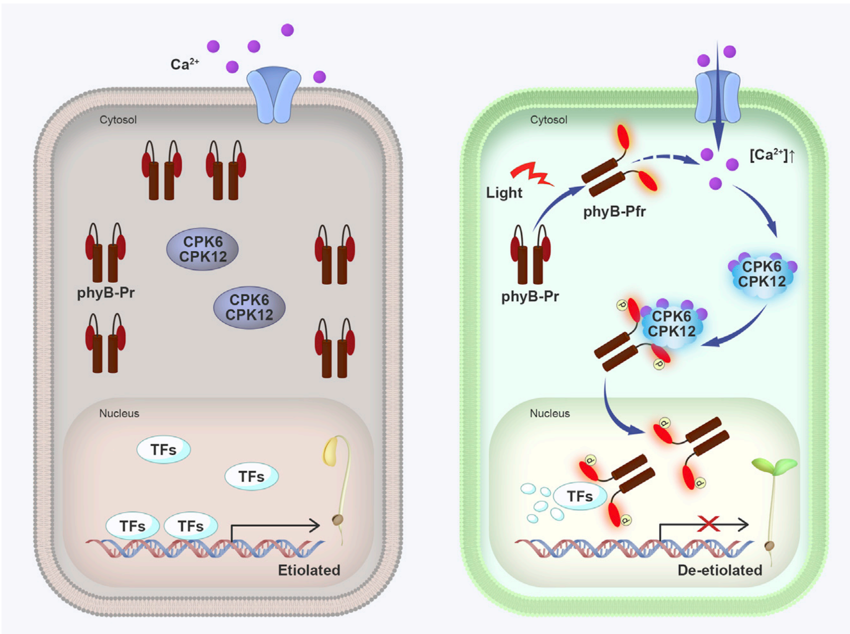

Figure 7. A Ca^{2+}-based sensory system controls red light signal transduction in etiolated seedlings upon initial light exposure

In etiolated seedlings, large amounts of photoreceptor phyB proteins as the Pr conformer exclusively accumulate in the cytosol, and Ca^{2+} sensors CPK6 and CPK12 (CPK6/12) are inactive. Red light exposure triggers an acute $[Ca^{2+}]_{cyt}$ increase through phyB to activate CPK6/12. In turn, the activated CPK6/12 interact with and phosphorylate the photo-activated Pfr conformer of phyB. This Ca^{2+}-sensor-directed phyB phosphorylation controls phyB nuclear translocation and transduces light signals from their perception directly to the nuclear events, including transcription factor (TF) degradation and gene expression alternations, thus achieves timely de-etiolation transition.

See also Figure S7.

Plants are faced with and have to distinguish and respond to various stimuli simultaneously. The prevailing notion is that the spatial and temporal kinetics of Ca^{2+} signals, known as calcium signatures, encode information about input stimuli to induce specific responses.[1] Observations showing that similar calcium signatures induce different responses or that different calcium signatures ultimately result in similar responses have also given rise to the hypothesis that calcium functions as "a chemical switch" in conjunction with other components to determine response specificity, which nevertheless remains largely speculative.[73,74] We reveal a regulatory loop of phyB-Ca^{2+}-CPK6/12-phyB centered in plant phototransduction. This loop is stimulated by and targets phyB, a receptor with the highest specificity in signaling pathways, and thus distinguishes its positive light signaling function from the Ca^{2+}-CPK regulation of other responses. The CPK6/12-phyB connection can be reconstituted by simultaneously applying external Ca^{2+} and red light irradiation *in vitro*, supporting the notion that calcium ions may act as generic activators with the specificity of responses being encrypted jointly with photoreceptors.

Regarding the events that occur between phyB activation and $[Ca^{2+}]_{cyt}$ increases, we speculate that cytosolic phyB activates plasma membrane calcium-permeable ion channels to trigger calcium influx upon red light exposure. This hypothesis is based on several lines of evidence: (1) red light stimulates $[Ca^{2+}]_{cyt}$ increases within seconds, and this response is blocked by a plasma membrane calcium channel inhibitor and mostly abolished in *phyB* mutant. (2) phyB has been previously shown to interact with plasma membrane-associated proteins such as phytochrome kinase substrate 1,[75,76] indicating the potential association between phyB and plasma membrane-localized proteins. (3) A series of microinjection experiments have suggested that heterotrimeric G proteins are the most upstream components of phytochrome signaling.[14,15] Therefore, it is likely that phyB by itself or through other intermediates, such as heterotrimeric G proteins, activates plasma membrane calcium channels. A future task is to identify the exact Ca^{2+} channels responsible for the red-light-stimulated Ca^{2+} influx, which further raises the question of how phyB activates the Ca^{2+} channels and what the connections between phytochromes, Ca^{2+} channels, and G proteins are.

Relatedly, photoreceptors photo1/2 were previously shown to be involved in blue-light-induced $[Ca^{2+}]$cyt increase.[77–79] Recent studies reported that the immune-receptor-associated kinase BIK1 directly interacts with and phosphorylates Ca^{2+}-permeable channels to trigger Ca^{2+} influx during pathogen attack,[9,80] and a receptor-channel trio activates Ca^{2+} signaling for pollen tube reception.[81] The direct interface of signal receptors and Ca^{2+}-based components might represent a universal mechanism for environment-sensing and signal transduction of plant cells.

Limitations of the study

In this study, we reveal a Ca^{2+}-centered regulatory loop in phyB phototransduction, providing a conceptual framework showing how the most versatile agent of Ca^{2+} is sensed and relayed into specific signaling outcomes. Although we show that red light stimulates increases in $[Ca^{2+}]_{cyt}$ via photoreceptor phyB, the mechanism of how phyB triggers Ca^{2+} influx needs further investigations. The $[Ca^{2+}]_{cyt}$ dynamics and the responsible Ca^{2+} channels in etiolated seedlings upon initial red light remain to be deciphered. In addition, we uncover that phosphorylation of phyB at S80/S106 represents a general mechanism controlling phyB nuclear import, where CPK6/12 play specific roles in etiolated seedlings upon initial light exposure. It is conceivable that multiple kinases are responsible for S80/106 phosphorylation of phyB under various conditions. Identifying those kinases would illuminate how plants employ diverse regulatory mechanisms of phosphorylation-determined phyB nuclear import to optimize their growth and development in accordance with varying environmental conditions.

STAR★METHODS

Detailed methods are provided in the online version of this paper and include the following:

- KEY RESOURCES TABLE
- RESOURCE AVAILABILITY
  - Lead contact
  - Materials availability
  - Data and code availability
- EXPERIMENTAL MODEL AND SUBJECT DETAILS
  - Plant Material and Growth Conditions
- METHOD DETAILS
  - Red light treatment
  - Ca^{2+} Signal imaging
  - Subcellular fluorescence imaging
  - Cytoplasm and nuclear separation assays
  - Immunoblot assays
  - RNA extraction and RT–qPCR
  - Firefly Luciferase Complementation Imaging (LCI) Assay
  - Protein expression and purification
  - Coimmunoprecipitation (Co-IP) Assays
  - In vitro Pull-down assays
  - In vitro phosphorylation assays
  - Immunoprecipitation Mass Spectrometry (IP-MS) Analyses
  - Sequence alignment
- QUANTIFICATION AND STATISTICAL ANALYSIS

SUPPLEMENTAL INFORMATION

Supplemental information can be found online at https://doi.org/10.1016/j.cell.2023.02.011.

ACKNOWLEDGMENTS

We greatly appreciate Drs. Akira Nagatani, Marc Knight, Jiankang Zhu, and Tsuyoshi Nakagawa for providing seeds and plasmids; and Drs. Yan Xue, Fang Yuan, and Kong Chen for their technical advice. We thank the National Center for Protein Sciences at Peking University in Beijing, China, particularly Xuemei Hao, Dong Liu, and Qi Zhang for their professional technical assistance with the mass spectrometry experiments. We thank the Analytical Instrumentation Center of Peking University and Wen Zhou for the technical help. We also thank Yue Li, Jing Li, Huan Li, Di Chen, Ying Wei, and Jiehui Huai for their experimental help. This work was supported by grants from the National Science Foundation of China (31621001 and 31822004) and Qidong-SLS Innovation Fund. H.S. was supported by the Support Project of High-Level Teachers in Beijing Municipal Universities in the Period of the 13th Five-Year Plan (CIT&TCD20190331).

AUTHOR CONTRIBUTIONS

S.Z. and H.S. designed the research. Y.Z., Y.P., M.L., Z.Y., and X.K. performed the experiments. S.Z., H.S., Y.Z., Y.P., and X.W.D. analyzed the data. S.Z. and H.S. wrote the paper.

DECLARATION OF INTERESTS

The authors declare no competing interests.

Received: October 15, 2021
Revised: August 23, 2022
Accepted: February 3, 2023
Published: March 16, 2023

REFERENCES

1. Berridge, M.J., Bootman, M.D., and Roderick, H.L. (2003). Calcium signalling: dynamics, homeostasis and remodelling. Nat. Rev. Mol. Cell Biol. *4*, 517–529. https://doi.org/10.1038/nrm1155.
2. Dodd, A.N., Kudla, J., and Sanders, D. (2010). The language of calcium signaling. Annu. Rev. Plant Biol. *61*, 593–620. https://doi.org/10.1146/annurev-arplant-070109-104628.
3. Kudla, J., Becker, D., Grill, E., Hedrich, R., Hippler, M., Kummer, U., Parniske, M., Romeis, T., and Schumacher, K. (2018). Advances and current challenges in calcium signaling. New Phytol. *218*, 414–431. https://doi.org/10.1111/nph.14966.
4. Knight, M.R., Campbell, A.K., Smith, S.M., and Trewavas, A.J. (1991). Transgenic plant aequorin reports the effects of touch and cold-shock and elicitors on cytoplasmic calcium. Nature *352*, 524–526. https://doi.org/10.1038/352524a0.
5. Allen, G.J., Chu, S.P., Harrington, C.L., Schumacher, K., Hoffmann, T., Tang, Y.Y., Grill, E., and Schroeder, J.I. (2001). A defined range of guard cell calcium oscillation parameters encodes stomatal movements. Nature *411*, 1053–1057. https://doi.org/10.1038/35082575.
6. Yuan, F., Yang, H., Xue, Y., Kong, D., Ye, R., Li, C., Zhang, J., Theprungsirikul, L., Shrift, T., Krichilsky, B., et al. (2014). OSCA1 mediates osmotic-stress-evoked Ca^{2+} increases vital for osmosensing in *Arabidopsis*. Nature *514*, 367–371. https://doi.org/10.1038/nature13593.
7. Toyota, M., Spencer, D., Sawai-Toyota, S., Jiaqi, W., Zhang, T., Koo, A.J., Howe, G.A., and Gilroy, S. (2018). Glutamate triggers long-distance, calcium-based plant defense signaling. Science *361*, 1112–1115. https://doi.org/10.1126/science.aat7744.
8. Jiang, Z.H., Zhou, X.P., Tao, M., Yuan, F., Liu, L.L., Wu, F.H., Wu, X.M., Xiang, Y., Niu, Y., Liu, F., et al. (2019). Plant cell-surface GIPC sphingolipids sense salt to trigger Ca^{2+} influx. Nature *572*, 341–346. https://doi.org/10.1038/s41586-019-1449-z.
9. Tian, W., Hou, C., Ren, Z., Wang, C., Zhao, F., Dahlbeck, D., Hu, S., Zhang, L., Niu, Q., Li, L., et al. (2019). A calmodulin-gated calcium channel links pathogen patterns to plant immunity. Nature *572*, 131–135. https://doi.org/10.1038/s41586-019-1413-y.
10. Pei, Z.M., Murata, Y., Benning, G., Thomine, S., Klüsener, B., Allen, G.J., Grill, E., and Schroeder, J.I. (2000). Calcium channels activated by hydrogen peroxide mediate abscisic acid signalling in guard cells. Nature *406*, 731–734. https://doi.org/10.1038/35021067.
11. Wayne, R., and Hepler, P.K. (1985). Red-light stimulates an increase in intracellular calcium in the spores of *Onoclea sensibilis*. Plant Physiol. *77*, 8–11. https://doi.org/10.1104/Pp.77.1.8.
12. Das, R., and Sopory, S.K. (1985). Evidence of regulation of calcium-uptake by phytochrome in maize protoplasts. Biochem. Biophys. Res. Commun. *128*, 1455–1460. https://doi.org/10.1016/0006-291x(85)91103-9.
13. Shacklock, P.S., Read, N.D., and Trewavas, A.J. (1992). Cytosolic free calcium mediates red light-induced photomorphogenesis. Nature *358*, 753–755. https://doi.org/10.1038/358753a0.
14. Neuhaus, G., Bowler, C., Kern, R., and Chua, N.H. (1993). Calcium/calmodulin-dependent and -independent phytochrome signal transduction pathways. Cell *73*, 937–952. https://doi.org/10.1016/0092-8674(93)90272-R.
15. Bowler, C., Neuhaus, G., Yamagata, H., and Chua, N.H. (1994). Cyclic GMP and calcium mediate phytochrome phototransduction. Cell *77*, 73–81. https://doi.org/10.1016/0092-8674(94)90236-4.
16. Fain, G.L., Hardie, R., and Laughlin, S.B. (2010). Phototransduction and the evolution of photoreceptors. Curr. Biol. *20*, R114–R124. https://doi.org/10.1016/j.cub.2009.12.006.

17. Huq, E., Al-Sady, B., Hudson, M., Kim, C., Apel, K., and Quail, P.H. (2004). Phytochrome-interacting factor 1 is a critical bHLH regulator of chlorophyll biosynthesis. Science *305*, 1937–1941. https://doi.org/10.1126/science.1099728.

18. Shi, H., Lyu, M., Luo, Y., Liu, S., Li, Y., He, H., Wei, N., Deng, X.W., and Zhong, S. (2018). Genome-wide regulation of light-controlled seedling morphogenesis by three families of transcription factors. Proc. Natl. Acad. Sci. USA *115*, 6482–6487. https://doi.org/10.1073/pnas.1803861115.

19. Quail, P.H. (2002). Phytochrome photosensory signalling networks. Nat. Rev. Mol. Cell Biol. *3*, 85–93. https://doi.org/10.1038/nrm728.

20. Chen, M., Chory, J., and Fankhauser, C. (2004). Light signal transduction in higher plants. Annu. Rev. Genet. *38*, 87–117. https://doi.org/10.1146/annurev.genet.38.072902.092259.

21. Hu, W., Franklin, K.A., Sharrock, R.A., Jones, M.A., Harmer, S.L., and Lagarias, J.C. (2013). Unanticipated regulatory roles for *Arabidopsis* phytochromes revealed by null mutant analysis. Proc. Natl. Acad. Sci. USA *110*, 1542–1547. https://doi.org/10.1073/pnas.1221738110.

22. Strasser, B., Sánchez-Lamas, M., Yanovsky, M.J., Casal, J.J., and Cerdán, P.D. (2010). *Arabidopsis thaliana* life without phytochromes. Proc. Natl. Acad. Sci. USA *107*, 4776–4781. https://doi.org/10.1073/pnas.0910446107.

23. Quail, P.H., Boylan, M.T., Parks, B.M., Short, T.W., Xu, Y., and Wagner, D. (1995). Phytochromes: photosensory perception and signal transduction. Science *268*, 675–680. https://doi.org/10.1126/science.7732376.

24. Rockwell, N.C., Su, Y.S., and Lagarias, J.C. (2006). Phytochrome structure and signaling mechanisms. Annu. Rev. Plant Biol. *57*, 837–858. https://doi.org/10.1146/annurev.arplant.56.032604.144208.

25. Schafer, E., and Bowle, C. (2002). Phytochrome-mediated photoperception and signal transduction in higher plants. EMBO Rep. *3*, 1042–1048. https://doi.org/10.1093/embo-reports/kvf222.

26. Klose, C., Venezia, F., Hussong, A., Kircher, S., Schäfer, E., and Fleck, C. (2015). Systematic analysis of how phytochrome B dimerization determines its specificity. Nat. Plants *1*, 15090. https://doi.org/10.1038/Nplants.2015.90.

27. Li, H., Burgie, E.S., Gannam, Z.T.K., Li, H.L., and Vierstra, R.D. (2022). Plant phytochrome B is an asymmetric dimer with unique signalling potential. Nature *604*, 127–133. https://doi.org/10.1038/s41586-022-04529-z.

28. Burgie, E.S., and Vierstra, R.D. (2014). Phytochromes: an atomic perspective on photoactivation and signaling. Plant Cell *26*, 4568–4583. https://doi.org/10.1105/tpc.114.131623.

29. Sakamoto, K., and Nagatani, A. (1996). Nuclear localization activity of phytochrome B. Plant J. *10*, 859–868. https://doi.org/10.1046/j.1365-313x.1996.10050859.x.

30. Kircher, S., Gil, P., Kozma-Bognár, L., Fejes, E., Speth, V., Husselstein-Muller, T., Bauer, D., Adám, E., Schäfer, E., and Nagy, F. (2002). Nucleocytoplasmic partitioning of the plant photoreceptors phytochrome A, B, C, D, and E is regulated differentially by light and exhibits a diurnal rhythm. Plant Cell *14*, 1541–1555. https://doi.org/10.1105/tpc.001156.

31. Leivar, P., and Quail, P.H. (2011). PIFs: pivotal components in a cellular signaling hub. Trends Plant Sci. *16*, 19–28. https://doi.org/10.1016/j.tplants.2010.08.003.

32. Lee, N., and Choi, G. (2017). Phytochrome-interacting factor from *Arabidopsis* to liverwort. Curr. Opin. Plant Biol. *35*, 54–60. https://doi.org/10.1016/j.pbi.2016.11.004.

33. Shi, H., Shen, X., Liu, R., Xue, C., Wei, N., Deng, X.W., and Zhong, S. (2016). The red light receptor phytochrome B directly enhances substrate-E3 ligase interactions to attenuate ethylene responses. Dev. Cell *39*, 597–610. https://doi.org/10.1016/j.devcel.2016.10.020.

34. Huq, E., Al-Sady, B., and Quail, P.H. (2003). Nuclear translocation of the photoreceptor phytochrome B is necessary for its biological function in seedling photomorphogenesis. Plant J. *35*, 660–664. https://doi.org/10.1046/j.1365-313X.2003.01836.x.

35. Fankhauser, C., and Chen, M. (2008). Transposing phytochrome into the nucleus. Trends Plant Sci. *13*, 596–601. https://doi.org/10.1016/j.tplants.2008.08.007.

36. Klose, C., Viczián, A., Kircher, S., Schäfer, E., and Nagy, F. (2015). Molecular mechanisms for mediating light-dependent nucleo/cytoplasmic partitioning of phytochrome photoreceptors. New Phytol. *206*, 965–971. https://doi.org/10.1111/nph.13207.

37. Harper, J.F., Sussman, M.R., Schaller, G.E., Putnam-Evans, C., Charbonneau, H., and Harmon, A.C. (1991). A calcium-dependent protein kinase with a regulatory domain similar to calmodulin. Science *252*, 951–954. https://doi.org/10.1126/science.1852075.

38. Liu, K.H., Niu, Y., Konishi, M., Wu, Y., Du, H., Sun Chung, H., Li, L., Boudsocq, M., McCormack, M., Maekawa, S., et al. (2017). Discovery of nitrate-CPK-NLP signalling in central nutrient-growth networks. Nature *545*, 311–316. https://doi.org/10.1038/nature22077.

39. Boudsocq, M., and Sheen, J. (2013). CDPKs in immune and stress signaling. Trends Plant Sci. *18*, 30–40. https://doi.org/10.1016/j.tplants.2012.08.008.

40. Cheng, S.H., Willmann, M.R., Chen, H.C., and Sheen, J. (2002). Calcium signaling through protein kinases. The *Arabidopsis* calcium-dependent protein kinase gene family. Plant Physiol. *129*, 469–485. https://doi.org/10.1104/pp.005645.

41. Mészáros, B., Erdos, G., and Dosztányi, Z. (2018). IUPred2A: context-dependent prediction of protein disorder as a function of redox state and protein binding. Nucleic Acids Res. *46*, W329–W337. https://doi.org/10.1093/nar/gky384.

42. Ruff, K.M., and Pappu, R.V. (2021). AlphaFold and implications for intrinsically disordered proteins. J. Mol. Biol. *433*, 167208. https://doi.org/10.1016/j.jmb.2021.167208.

43. Chen, D., Lyu, M., Kou, X., Li, J., Yang, Z., Gao, L., Li, Y., Fan, L.M., Shi, H., and Zhong, S. (2022). Integration of light and temperature sensing by liquid-liquid phase separation of phytochrome B. Mol. Mol. Cell *82*, 3015–3029.e6. https://doi.org/10.1016/j.molcel.2022.05.026.

44. Kircher, S., Kozma-Bognar, L., Kim, L., Adam, E., Harter, K., Schafer, E., and Nagy, F. (1999). Light quality-dependent nuclear import of the plant photoreceptors phytochrome A and B. Plant Cell *11*, 1445–1456. https://doi.org/10.1105/tpc.11.8.1445.

45. Hisada, A., Hanzawa, H., Weller, J.L., Nagatani, A., Reid, J.B., and Furuya, M. (2000). Light-induced nuclear translocation of endogenous pea phytochrome A visualized by immunocytochemical procedures. Plant Cell *12*, 1063–1078. https://doi.org/10.1105/tpc.12.7.1063.

46. Saijo, Y., Zhu, D., Li, J., Rubio, V., Zhou, Z., Shen, Y., Hoecker, U., Wang, H., and Deng, X.W. (2008). *Arabidopsis* COP1/SPA1 complex and FHY1/FHY3 associate with distinct phosphorylated forms of phytochrome A in balancing light signaling. Mol. Cell *31*, 607–613. https://doi.org/10.1016/j.molcel.2008.08.003.

47. Zhang, Y., Mayba, O., Pfeiffer, A., Shi, H., Tepperman, J.M., Speed, T.P., and Quail, P.H. (2013). A quartet of PIF bHLH factors provides a transcriptionally centered signaling hub that regulates seedling morphogenesis through differential expression-patterning of shared target genes in *Arabidopsis*. PLoS Genet. *9*, e1003244. https://doi.org/10.1371/journal.pgen.1003244.

48. Pfeiffer, A., Shi, H., Tepperman, J.M., Zhang, Y., and Quail, P.H. (2014). Combinatorial complexity in a transcriptionally centered signaling hub in *Arabidopsis*. Mol. Plant *7*, 1598–1618. https://doi.org/10.1093/Mp/Ssu087.

49. Willige, B.C., Zander, M., Yoo, C.Y., Phan, A., Garza, R.M., Wanamaker, S.A., He, Y.P., Nery, J.R., Chen, H.M., Chen, M., et al. (2021). PHYTOCHROME-INTERACTING FACTORs trigger environmentally responsive chromatin dynamics in plants. Nat. Genet. *53*, 955–961. https://doi.org/10.1038/s41588-021-00882-3.

50. Nito, K., Wong, C.C., Yates, J.R., 3rd, and Chory, J. (2013). Tyrosine phosphorylation regulates the activity of phytochrome photoreceptors. Cell Rep. *3*, 1970–1979. https://doi.org/10.1016/j.celrep.2013.05.006.

51. Viczián, A., Ádám, É., Staudt, A.M., Lambert, D., Klement, E., Romero Montepaone, S., Hiltbrunner, A., Casal, J., Schäfer, E., Nagy, F., et al. (2020). Differential phosphorylation of the N-terminal extension regulates phytochrome B signaling. New Phytol. *225*, 1635–1650. https://doi.org/10.1111/nph.16243.

52. Medzihradszky, M., Bindics, J., Ádám, É., Viczián, A., Klement, É., Lorrain, S., Gyula, P., Mérai, Z., Fankhauser, C., Medzihradszky, K.F., et al. (2013). Phosphorylation of phytochrome B inhibits light-induced signaling via accelerated dark reversion in *Arabidopsis*. Plant Cell *25*, 535–544. https://doi.org/10.1105/tpc.112.106898.

53. Van Buskirk, E.K., Reddy, A.K., Nagatani, A., and Chen, M. (2014). Photobody localization of phytochrome B is tightly correlated with prolonged and light-dependent inhibition of hypocotyl elongation in the dark. Plant Physiol. *165*, 595–607. https://doi.org/10.1104/pp.114.236661.

54. Huang, H., McLoughlin, K.E., Sorkin, M.L., Burgie, E.S., Bindbeutel, R.K., Vierstra, R.D., and Nusinow, D.A. (2019). PCH1 regulates light, temperature, and circadian signaling as a structural component of phytochrome B-photobodies in *Arabidopsis*. Proc. Natl. Acad. Sci. USA *116*, 8603–8608. https://doi.org/10.1073/pnas.1818217116.

55. Mathews, S. (2010). Evolutionary studies illuminate the structural-functional model of plant phytochromes. Plant Cell *22*, 4–16. https://doi.org/10.1105/tpc.109.072280.

56. Shen, H., Zhu, L., Castillon, A., Majee, M., Downie, B., and Huq, E. (2008). Light-induced phosphorylation and degradation of the negative regulator PHYTOCHROME-INTERACTING FACTOR1 from *Arabidopsis* depend upon its direct physical interactions with photoactivated phytochromes. Plant Cell *20*, 1586–1602. https://doi.org/10.1105/tpc.108.060020.

57. Al-Sady, B., Ni, W., Kircher, S., Schäfer, E., and Quail, P.H. (2006). Photoactivated phytochrome induces rapid PIF3 phosphorylation prior to proteasome-mediated degradation. Mol. Cell *23*, 439–446. https://doi.org/10.1016/j.molcel.2006.06.011.

58. Deng, X.W. (1994). Fresh view of light signal transduction in plants. Cell *76*, 423–426. https://doi.org/10.1016/0092-8674(94)90107-4.

59. Millar, A.J., McGrath, R.B., and Chua, N.H. (1994). Phytochrome phototransduction pathways. Annu. Rev. Genet. *28*, 325–349. https://doi.org/10.1146/annurev.ge.28.120194.001545.

60. Ni, M., Tepperman, J.M., and Quail, P.H. (1998). PIF3, a phytochrome-interacting factor necessary for normal photoinduced signal transduction, is a novel basic helix-loop-helix protein. Cell *95*, 657–667. https://doi.org/10.1016/s0092-8674(00)81636-0.

61. Chen, M., Galvão, R.M., Li, M., Burger, B., Bugea, J., Bolado, J., and Chory, J. (2010). *Arabidopsis* HEMERA/pTAC12 initiates photomorphogenesis by phytochromes. Cell *141*, 1230–1240. https://doi.org/10.1016/j.cell.2010.05.007.

62. Park, E., Kim, Y., and Choi, G. (2018). Phytochrome B requires PIF degradation and sequestration to induce light responses across a wide range of light conditions. Plant Cell *30*, 1277–1292. https://doi.org/10.1105/tpc.17.00913.

63. Oh, E., Kim, J., Park, E., Kim, J.I., Kang, C., and Choi, G. (2004). PIL5, a phytochrome-interacting basic helix-loop-helix protein, is a key negative regulator of seed germination in *Arabidopsis thaliana*. Plant Cell *16*, 3045–3058. https://doi.org/10.1105/tpc.104.025163.

64. Su, Y.S., and Lagarias, J.C. (2007). Light-independent phytochrome signaling mediated by dominant GAF domain tyrosine mutants of *Arabidopsis* phytochromes in transgenic plants. Plant Cell *19*, 2124–2139. https://doi.org/10.1105/tpc.107.051516.

65. Taira, N., Nihira, K., Yamaguchi, T., Miki, Y., and Yoshida, K. (2007). DYRK2 is targeted to the nucleus and controls p53 via Ser46 phosphorylation in the apoptotic response to DNA damage. Mol. Cell *25*, 725–738. https://doi.org/10.1016/j.molcel.2007.02.007.

66. D'Orazi, G., Cecchinelli, B., Bruno, T., Manni, I., Higashimoto, Y., Saito, S., Gostissa, M., Coen, S., Marchetti, A., Del Sal, G., et al. (2002). Homeodomain-interacting protein kinase-2 phosphorylates p53 at Ser 46 and mediates apoptosis. Nat. Cell Biol. *4*, 11–19. https://doi.org/10.1038/ncb714.

67. Lyu, M., Shi, H., Li, Y., Kuang, K., Yang, Z., Li, J., Chen, D., Kou, X., and Zhong, S. (2019). Oligomerization and photo-deoligomerization of HOOKLESS1 controls plant differential cell growth. Dev. Cell *51*, 78-88.e73. https://doi.org/10.1016/j.devcel.2019.08.007.

68. Hiltbrunner, A., Viczián, A., Bury, E., Tscheuschler, A., Kircher, S., Tóth, R., Honsberger, A., Nagy, F., Fankhauser, C., and Schäfer, E. (2005). Nuclear accumulation of the phytochrome A photoreceptor requires FHY1. Curr. Biol. *15*, 2125–2130. https://doi.org/10.1016/j.cub.2005.10.042.

69. Zhou, Q., Hare, P.D., Yang, S.W., Zeidler, M., Huang, L.F., and Chua, N.H. (2005). FHL is required for full phytochrome A signaling and shares overlapping functions with FHY1. Plant J. *43*, 356–370. https://doi.org/10.1111/j.1365-313X.2005.02453.x.

70. Pfeiffer, A., Kunkel, T., Hiltbrunner, A., Neuhaus, G., Wolf, I., Speth, V., Adam, E., Nagy, F., and Schäfer, E. (2009). A cell-free system for light-dependent nuclear import of phytochrome. Plant J. *57*, 680–689. https://doi.org/10.1111/j.1365-313X.2008.03721.x.

71. Genoud, T., Schweizer, F., Tscheuschler, A., Debrieux, D., Casal, J.J., Schäfer, E., Hiltbrunner, A., and Fankhauser, C. (2008). FHY1 mediates nuclear import of the light-activated phytochrome A photoreceptor. PLoS Genet. *4*, e1000143. https://doi.org/10.1371/journal.pgen.1000143.

72. Chen, M., Tao, Y., Lim, J., Shaw, A., and Chory, J. (2005). Regulation of phytochrome B nuclear localization through light-dependent unmasking of nuclear-localization signals. Curr. Biol. *15*, 637–642. https://doi.org/10.1016/j.cub.2005.02.028.

73. Scrase-Field, S.A.M.G., and Knight, M.R. (2003). Calcium: just a chemical switch? Curr. Opin. Plant Biol. *6*, 500–506. https://doi.org/10.1016/S1369-5266(03)00091-8.

74. Edel, K.H., Marchadier, E., Brownlee, C., Kudla, J., and Hetherington, A.M. (2017). The evolution of calcium-based signalling in plants. Curr. Biol. *27*, R667–R679. https://doi.org/10.1016/j.cub.2017.05.020.

75. Fankhauser, C., Yeh, K.C., Lagarias, J.C., Zhang, H., Elich, T.D., and Chory, J. (1999). PKS1, a substrate phosphorylated by phytochrome that modulates light signaling in *Arabidopsis*. Science *284*, 1539–1541. https://doi.org/10.1126/science.284.5419.1539.

76. Lariguet, P., Schepens, I., Hodgson, D., Pedmale, U.V., Trevisan, M., Kami, C., de Carbonnel, M., Alonso, J.M., Ecker, J.R., Liscum, E., and Fankhauser, C. (2006). PHYTOCHROME kinase SUBSTRATE 1 is a phototropin 1 binding protein required for phototropism. Proc. Natl. Acad. Sci. USA *103*, 10134–10139. https://doi.org/10.1073/pnas.0603799103.

77. Babourina, O., Newman, I., and Shabala, S. (2002). Blue light-induced kinetics of H^+ and Ca^{2+} fluxes in etiolated wild-type and phototropin-mutant *Arabidopsis* seedlings. Proc. Natl. Acad. Sci. USA *99*, 2433–2438. https://doi.org/10.1073/pnas.042294599.

78. Stoelzle, S., Kagawa, T., Wada, M., Hedrich, R., and Dietrich, P. (2003). Blue light activates calcium-permeable channels in *Arabidopsis* mesophyll cells via the phototropin signaling pathway. Proc. Natl. Acad. Sci. USA *100*, 1456–1461. https://doi.org/10.1073/pnas.0333408100.

79. Harada, A., Sakai, T., and Okada, K. (2003). phot1 and phot2 mediate blue light-induced transient increases in cytosolic Ca^{2+} differently in *Arabidopsis* leaves. Proc. Natl. Acad. Sci. USA *100*, 8583–8588. https://doi.org/10.1073/pnas.1336802100.

80. Thor, K., Jiang, S.S., Michard, E., George, J., Scherzer, S., Huang, S.G., Dindas, J., Derbyshire, P., Leitão, N., DeFalco, T.A., et al. (2020). The calcium-permeable channel OSCA1.3 regulates plant stomatal immunity. Nature *585*, 569–573. https://doi.org/10.1038/s41586-020-2702-1.

81. Gao, Q., Wang, C., Xi, Y., Shao, Q., Li, L., and Luan, S. (2022). A receptor-channel trio conducts Ca^{2+} signalling for pollen tube reception. Nature *607*, 534–539. https://doi.org/10.1038/s41586-022-04923-7.

82. Zhong, S., Zhao, M., Shi, T., Shi, H., An, F., Zhao, Q., and Guo, H. (2009). EIN3/EIL1 cooperate with PIF1 to prevent photo-oxidation and to promote greening of *Arabidopsis* seedlings. Proc. Natl. Acad. Sci. USA *106*, 21431–21436. https://doi.org/10.1073/pnas.0907670106.

83. Zhong, S., Shi, H., Xue, C., Wang, L., Xi, Y., Li, J., Quail, P.H., Deng, X.W., and Guo, H. (2012). A molecular framework of light-controlled phytohormone action in *Arabidopsis*. Curr. Biol. *22*, 1530–1535. https://doi.org/10.1016/j.cub.2012.06.039.

84. Matsushita, T., Mochizuki, N., and Nagatani, A. (2003). Dimers of the N-terminal domain of phytochrome B are functional in the nucleus. Nature *424*, 571–574. https://doi.org/10.1038/nature01837.

85. Alonso, J.M., Stepanova, A.N., Leisse, T.J., Kim, C.J., Chen, H., Shinn, P., Stevenson, D.K., Zimmerman, J., Barajas, P., Cheuk, R., et al. (2003). Genome-wide insertional mutagenesis of *Arabidopsis thaliana*. Science *301*, 653–657. https://doi.org/10.1126/science.1086391.

86. Yoshida, Y., Sarmiento-Mañús, R., Yamori, W., Ponce, M.R., Micol, J.L., and Tsukaya, H. (2018). The *Arabidopsis phyB-9* mutant has a second-site mutation in the *VENOSA4* gene that alters chloroplast size, photosynthetic traits, and leaf growth. Plant Physiol. *178*, 3–6. https://doi.org/10.1104/pp.18.00764.

87. Zhang, Z.J., Mao, Y.F., Ha, S., Liu, W.S., Botella, J.R., and Zhu, J.K. (2016). A multiplex CRISPR/Cas9 platform for fast and efficient editing of multiple genes in *Arabidopsis*. Plant Cell Rep. *35*, 1519–1533. https://doi.org/10.1007/s00299-015-1900-z.

88. Feng, Z.Y., Zhang, B.T., Ding, W.N., Liu, X.D., Yang, D.L., Wei, P.L., Cao, F.Q., Zhu, S.H., Zhang, F., Mao, Y.F., and Zhu, J.K. (2013). Efficient genome editing in plants using a CRISPR/Cas system. Cell Res. *23*, 1229–1232. https://doi.org/10.1038/cr.2013.114.

89. Nakagawa, T., Suzuki, T., Murata, S., Nakamura, S., Hino, T., Maeo, K., Tabata, R., Kawai, T., Tanaka, K., Niwa, Y., et al. (2007). Improved Gateway binary vectors: high-performance vectors for creation of fusion constructs in transgenic analysis of plants. Biosci. Biotechnol. Biochem. *71*, 2095–2100. https://doi.org/10.1271/bbb.70216.

90. Leivar, P., Monte, E., Oka, Y., Liu, T., Carle, C., Castillon, A., Huq, E., and Quail, P.H. (2008). Multiple phytochrome-interacting bHLH transcription factors repress premature seedling photomorphogenesis in darkness. Curr. Biol. *18*, 1815–1823. https://doi.org/10.1016/j.cub.2008.10.058.

91. Knight, H., Trewavas, A.J., and Knight, M.R. (1996). Cold calcium signaling in *Arabidopsis* involves two cellular pools and a change in calcium signature after acclimation. Plant Cell *8*, 489–503. https://doi.org/10.1105/tpc.8.3.489.

92. Liu, X., Liu, R., Li, Y., Shen, X., Zhong, S., and Shi, H. (2017). EIN3 and PIF3 form an interdependent module that represses chloroplast development in buried seedlings. Plant Cell *29*, 3051–3067. https://doi.org/10.1105/tpc.17.00508.

93. Ni, W., Xu, S.L., Tepperman, J.M., Stanley, D.J., Maltby, D.A., Gross, J.D., Burlingame, A.L., Wang, Z.Y., and Quail, P.H. (2014). A mutually assured destruction mechanism attenuates light signaling in *Arabidopsis*. Science *344*, 1160–1164. https://doi.org/10.1126/science.1250778.

94. Lo, H.C., and Hollingsworth, N.M. (2011). Using the semi-synthetic epitope system to identify direct substrates of the meiosis-specific budding yeast kinase, Mek1. Methods Mol. Biol. *745*, 135–149. https://doi.org/10.1007/978-1-61779-129-1_9.

95. Olsen, J.V., Ong, S.E., and Mann, M. (2004). Trypsin cleaves exclusively C-terminal to arginine and lysine residues. Mol. Cell. Proteomics *3*, 608–614. https://doi.org/10.1074/mcp.T400003-MCP200.

96. Ni, W., Xu, S.L., Chalkley, R.J., Pham, T.N., Guan, S., Maltby, D.A., Burlingame, A.L., Wang, Z.Y., and Quail, P.H. (2013). Multisite light-induced phosphorylation of the transcription factor PIF3 is necessary for both its rapid degradation and concomitant negative feedback modulation of photoreceptor phyB levels in *Arabidopsis*. Plant Cell *25*, 2679–2698. https://doi.org/10.1105/tpc.113.112342.

97. Wang, Q., Barshop, W.D., Bian, M., Vashisht, A.A., He, R.Q., Yu, X.H., Liu, B., Nguyen, P., Liu, X.M., Zhao, X.Y., et al. (2015). The blue light-dependent phosphorylation of the CCE domain determines the photosensitivity of *Arabidopsis* CRY2. Mol. Plant *8*, 631–643. https://doi.org/10.1016/j.molp.2015.03.005.

STAR★METHODS

KEY RESOURCES TABLE

REAGENT or RESOURCE	SOURCE	IDENTIFIER
Antibodies		
GFP	Abcam	Cat# ab13970; RRID:AB_300798
Actin	Sigma-Aldrich	Cat# A0480; RRID:AB_476670
HSP	Thermo Fisher	Cat# MA1-10372; RRID:AB_11155433
histone	Sigma-Aldrich	Cat# H0164; RRID:AB_532248
MBP	New England Biolabs	Cat# E8032; RRID:AB_1559730
Myc	Sigma-Aldrich	Cat# M4439; RRID:AB_439694
HA	Cell Signaling Technology	Cat# C29F4
RPN6	Abmart	Cat# X-Q9LP45-N
tubulin	Sigma-Aldrich	Cat# T8203; RRID:AB_1841230
phyB	Shi et al.[33]	N/A
PIF1	This paper	N/A
PIF3	Liu et al.[38]	N/A
phyA	Saijo et al.[46]	N/A
thiophosphate ester	Epitomics	Cat# 2686-1
Bacterial and virus strains		
DH5 competent cell	Tiangen	N/A
GV3101	Transgen	N/A
BL21	Tiangen	N/A
Chemicals, peptides, and recombinant proteins		
EGTA	Sigma-Aldrich	Cat# E3889
$LaCl_3$	Sigma-Aldrich	Cat# 449830
Murashige and Skoog Basal Medium	Sigma-Aldrich	Cat# M0404
cOmplete, EDTA-free Protease Inhibitor Cocktail	Roche	Cat# 4693132001
Phosophatase Inhibitor Cocktail	Roche	Cat# 4906837001
PMSF	American Bioanalytical	Cat# AB01620
Glycerol	American Bioanalytical	Cat# AB00751
Ammonium persulfate	Sigma-Aldrich	Cat# A3678
Triton X-100	American Bioanalytical	Cat# AB02025
Acrylamide/Bis-acrylamide	Sigma-Aldrich	Cat# A3669
Ammonium persulfate	Sigma-Aldrich	Cat# A3678
N,N,N,N -Tetramethylethylenediamine	Sigma-Aldrich	Cat# M2670
ECL Western Blotting Detection Reagents	GE Healthcare	Cat# RPN2209
2-mercaptoethanol	Sigma-Aldrich	Cat# M3148
Coelenterazine	NanoLight Technologies	Cat# 303-10mg
DTT	American Bioanalytical	Cat# AB00490
D-luciferin	Promega	Cat# E1500
6-Fu-ATPγS	BioLog	Cat# F008-05
ATP	Actis	Cat# ACS1374
PNBM	Abcam	Cat# Ab138910
Ni-NTA agarose	Qiagen	Cat# 302010
GFP Trap Agarose	ChromoTeK	Cat# GTA-20
EZview Red c-Myc-Agarose	Sigma-Aldrich	Cat# E6654-1ML
Critical commercial assays		
A spectrum Plant Total RNA Kit	Sigma-Aldrich	Cat# 74904

(*Continued on next page*)

Continued		
REAGENT or RESOURCE	SOURCE	IDENTIFIER
ReverTra Ace qPCR RT Master Mix	TOYOBO	Cat# FSQ-201
SYBR Green Mix	Takara	Cat# RR42LR
Fast Mutagenesis system	Transgen	Cat# FM111
Experimental models: Organisms/strains		
Arabidopsis cpk6	*Arabidopsis* Biological Resource Center	SALK_025460C
Arabidopsis cpk12	*Arabidopsis* Biological Resource Center	SALK_090011C
Arabidopsis pif1	Zhong et al.[82]	N/A
Arabidopsis pif3	Zhong et al.[83]	N/A
Arabidopsis cpk6 cpk12	This paper	N/A
Arabidopsis phyB-9 cpk6 cpk12	This paper	N/A
Arabidopsis 35S:phyB-GFP/phyB-5 (PBG)	Matsushita et al.[84]	N/A
Arabidopsis AEQ	Knight et al.[4]	N/A
Arabidopsis phyB-9	ABRC	CS6217
Arabidopsis AEQ/*phyB-9*	This paper	N/A
Arabidopsis PBG/*cpk6 cpk12-Cas*	This paper	N/A
Arabidopsis 35S:CPK6-*Myc (CPK6-Myc)*	This paper	N/A
Arabidopsis 35S:CPK12-*Myc (CPK12-Myc)*	This paper	N/A
Arabidopsis 35S:phyB-YFP/phyB-9 (phyB-WT)	This paper	N/A
Arabidopsis 35S:phyB-NLS-YFP/phyB-9 (*phyB-WT-NLS*)	This paper	N/A
Arabidopsis 35S:phyB-2A-YFP/phyB-9 (*phyB-2A*)	This paper	N/A
Arabidopsis 35S:phyB-2A-NLS-YFP/phyB-9 (*phyB-2A-NLS*)	This paper	N/A
Arabidopsis 35S:phyB-2D-YFP/phyB-9 (*phyB-2D*)	This paper	N/A
Arabidopsis 35S:phyB-2D-NLS-YFP/phyB-9 (*phyB-2D-NLS*)	This paper	N/A
Arabidopsis 35S:phyB-NLS-YFP/cpk6 cpk12-Cas (*phyB-NLS/cpk6 cpk12-Cas*)	This paper	N/A
Oligonucleotides		
Primers are listed in Table S1	This paper	N/A
Recombinant DNA		
pET28a-phyBN	This paper	N/A
pET28a-phyBN-2A	This paper	N/A
pcDNA3.1- PIF1-Myc	This paper	N/A
pcDNA3.1- PIF3-Myc	This paper	N/A
pcDNA3.1-phyB-2A-YFP	This paper	N/A
pcDNA3.1-phyD-HA	This paper	N/A
pcDNA3.1-phyE-YFP	This paper	N/A
pcDNA3.1-CPK6-Myc	This paper	N/A
pcDNA3.1- CPK12-Myc	This paper	N/A
pFastbacHT B-phyB	This paper	N/A
pENTR4-phyB-WT	This paper	N/A
pENTR4-phyB-2A	This paper	N/A
pENTR4-phyB-2D	This paper	N/A
pENTR4-CPK6	This paper	N/A

(*Continued on next page*)

Continued

REAGENT or RESOURCE	SOURCE	IDENTIFIER
pENTR4-CPK12	This paper	N/A
pGWB-617-CPK6	This paper	N/A
pGWB-617-CPK12	This paper	N/A
pGWB-641-phyB-WT	This paper	N/A
pGWB-641-phyB-2A	This paper	N/A
pGWB-641-phyB-2D	This paper	N/A
pGWB-641-phyB-WT-NLS	This paper	N/A
pGWB-641-phyB-2A-NLS	This paper	N/A
pGWB-641-phyB-2D-NLS	This paper	N/A
pGWB-641-phyD-WT	This paper	N/A
pGWB-641-phyD-2A	This paper	N/A
pGWB-641-phyD-2A-NLS	This paper	N/A
pGWB-641-phyE-WT	This paper	N/A
pGWB-641-phyE-2A	This paper	N/A
pGWB-641-phyE-2A-NLS	This paper	N/A
pCAMBIA1300-phyB-LUC^n	This paper	N/A
pCAMBIA1300-CPK-LUC^c	This paper	N/A
pCAMBIA1300-phyD-LUC^n	This paper	N/A
pCAMBIA1300-phyE-LUC^n	This paper	N/A
pMAL-CPK6	This paper	N/A
pMAL-CPK12	This paper	N/A
Software and algorithms		
ImageJ	NIH,USA	http://rsb.info/nih/gov/ij
MEGA	Molecular Evolutionary Genetics Analysis	https://megasoftware.net
IndiGo	Berthold Technologies	https://www.berthold.cn/bioanalytic
Proteome Discoverer™	Thermo Fisher Scientific	https://www.thermofisher.cn/order/catalog/product/OPTON-30810
MAFFT	Osaka University	https://mafft.cbrc.jp/alignment/server/

RESOURCE AVAILABILITY

Lead contact

Further information and requests for resources and reagents should be directed to and will be fulfilled by the lead contact, Shangwei Zhong (shangwei.zhong@pku.edu.cn).

Materials availability

Constructs and unique reagents generated in this study will be available from the lead contact upon request.

Data and code availability

- All data reported in this paper are available from the lead contact upon request.
- This paper does not report original code.
- Any additional information required to reanalyze the data reported in this paper is available from the lead contact upon request.

EXPERIMENTAL MODEL AND SUBJECT DETAILS

Plant Material and Growth Conditions

The main ecotype of *Arabidopsis thaliana* used in this study was Columbia (Col-0), excepting that *35S:phyB-GFP* (PBG) was generated in the Landsberg *erecta* (L*er*-0) background. PBG, *phyB-9*, AEQ (Col-0 expressing aequorin), *pif1* and *pif3* were previously reported.[4,61,82–84] The *Arabidopsis* T-DNA insertion lines *cpk6* (SALK_025460C) and *cpk12* (SALK_090011C) were obtained from *Arabidopsis* Biological Resource Center, and homozygosity was confirmed by PCR.[85] The *cpk6 cpk12* and *phyB-9 cpk6 cpk12* mutants were obtained by genetic crossing and confirmed by PCR. AEQ/*phyB-9* was obtained by genetic crossing AEQ with *phyA-211 phyB-9* and confirmed by sequencing along with antibiotic resistance selection (Methods S1).[86] The CPK6/12 mutations in PBG/*cpk6 cpk12-Cas* and *cpk6 cpk12-Cas* were generated by using the CRISPR/Cas9 system in the PBG and Col-0 background, respectively.[87] sgRNAs targeting the *CPK6* and *CPK12* locus obtained from the website https://crispr.dbcls.jp was cloned into the binary vector pEx-ptAtUBQ-Cas9.[88] The coding region of *phyB* amplified from *Arabidopsis* cDNA by PCR was cloned into the pENTR4 vector (Invitrogen) to generate the pENTR4-phyB-WT construct. pENTR4-phyB-2A/2D constructs were generated by site-directed mutagenesis (Transgen, China). All entry clones were inserted into pGWB-641,[89] and transformed into *phyB-9* mutant. *phyB-WT*#14, *phyB-2A*#30, and *phyB-2D*#10, expressing comparable levels of phyB-YFP proteins, were used unless otherwise specified. The coding region of *CPK6* or *CPK12* amplified from *Arabidopsis* cDNA by PCR was cloned into pGWB-617 for generating the 35S:CPK6-*Myc* and 35S:CPK12-*Myc* plants.[89] The floral-dip method of *Agrobacterium tumefaciens* (GV3101) transformation was used for *Arabidopsis* transformation.

Seeds were surface-sterilized by using sterilization buffer containing 75% ethanol and 0.1% Triton X-100 and were then plated on half-strength MS medium (2.2 g/L MS salts, 5 g/L sucrose, and 8 g/L agar, pH=5.7). The plated seeds were imbibed in darkness at 4 °C for 3 days and were then illuminated under white light for 6 h to induce germination before incubation under the indicated conditions. For dark incubation, the seeds were irradiated with 50 μmol m^{-2} s^{-1} far-red light for 5 min and were then incubated in darkness.[90] For red light treatment, 30 μmol m^{-2} s^{-1} red light was supplied, unless otherwise specified. *Arabidopsis* seedlings were grown at 22 °C in a growth chamber. Adult *Arabidopsis* plants were grown under a 16 h/8 h day/night photoperiod at 22 °C. For chemical treatment, the seedlings were treated with 20 mM EGTA, 10 mM $LaCl_3$ or 2 mM $CaCl_2$, unless otherwise specified.[38,91]

METHOD DETAILS

Red light treatment

To investigate the effects of red light on calcium signaling, we used a light-emitting diode (LED) red light source, which has a narrow spectral output that peaks at approximately 670 nm, with a 10 nm half bandwidth (Methods S2). To examine whether the autofluorescence of photosynthetic pigments was induced or not by our narrow band red light source, we additionally detected the signals of WT (with coelentrazine pretreatment) and AEQ (without coelentrazine pretreatment) upon red light irradiance. No measurable luminescence above background was detected in these controls. Therefore, the luminescence signal we detected is not due to fluorescence from the photosynthetic pigments.

Ca^{2+} Signal imaging

Aequorin bioluminescence-based Ca^{2+} signal determination was performed as previously described with some modifications.[6,9] AEQ seedlings were grown on 1/2 MS medium in the dark for 3 days. Thereafter, the seedlings were evenly sprayed with 80 μM coelenterazine (NanoLight Technologies) and incubated in the dark overnight. For light treatment, 30 s of 300 μmol m^{-2} s^{-1} red light, 10 μmol m^{-2} s^{-1} far-red light, or 10 μmol m^{-2} s^{-1} green light exposure was performed. Aequorin bioluminescence images were recorded with 3 min exposure time using BERTHOLD TECHNOLOGIES LB985, and the bioluminescence intensity was quantified using IndiGo (Berthold Technologies). Luminescence change rate (ΔL/L0) was calculated as: the luminescence intensity of the light-irradiated sample minus that of the dark control sample and then was divided by the luminescence intensity of the dark control sample. For the time-course analysis of Ca^{2+} signals, AEQ transgenic seedlings were grown under white light for 9 days and were then irradiated with far-red light to inactivate phytochrome. Individual seedlings were transferred to one well of 96-well plates containing 100 μl 0.1‰ Triton X-100 supplemented with 20 μM coelenterazine and were then incubated in the dark overnight. For light treatment, 1 min of 300 μmol m^{-2} s^{-1} red light exposure was performed. Luminescence (L) was recorded at intervals of 5 s using BERTHOLD TECHNOLOGIES Multimode Reader LB942. At the end of the experiment, the total remaining aequorin was discharged using 1 M $CaCl_2$ in 10% (v/v) ethanol, and the $[Ca^{2+}]_{cyt}$ was calculated according to the formula pCa = 0.332588 × (-log κ) + 5.5593 described previously.[91]

Subcellular fluorescence imaging

For experiments involving *Arabidopsis* seedlings, transgenic *Arabidopsis* plants expressing phyB-GFP or phyB-YFP were grown in the dark for 3 days and were then irradiated with red light for 2 h unless otherwise specified. Hypocotyl and cotyledon cells were observed with a confocal laser scanning microscope (Carl Zeiss, LSM520 Meta). GFP fluorescence was excited at 488 nm, and YFP fluorescence was excited at 514 nm.

For experiments involving tobacco leaves, *Agrobacterium tumefaciens* carrying the indicated constructs were infiltrated into *Nicotiana benthamiana* leaves. After 2 days of growth, dark-adapted tobacco plants were irradiated by far-red light for 30 min and then were incubated in darkness overnight before observation. YFP fluorescence from tobacco epidermal cells was observed with a confocal laser scanning microscope (Carl Zeiss, LSM520 Meta) at an excitation wavelength of 514 nm.

Cytoplasm and nuclear separation assays

Seedlings were grown in the dark for 3 days and were then maintained in darkness or irradiated with red light for 2 h unless otherwise specified. Approximately 0.5 g of seedling samples were harvested and ground to fine powder in liquid nitrogen under dim green light in a dark room. Two milliliters of cold lysis buffer (20 mM Tris-HCl, pH=7.4, 20 mM KCl, 2 mM EDTA, 2.5 mM $MgCl_2$, 250 mM sucrose, 25% glycerol, 30 mM β-mercaptoethanol, 1 mM PMSF, and a Roche protease inhibitor cocktail) was added to the powder. The homogenate filtered through a nylon mesh was centrifuged at 1500 g for 20 min and then at 12000 g for 20 min at 4 °C, and the clear supernatant was collected as the cytoplasmic fraction. The pellet was suspended by pipetting it with 3 ml washing buffer (20 mM Tris-HCl, pH=7.4, 150 mM NaCl, 10 mM $MgCl_2$, and 0.5 mM EDTA), and this suspension was centrifuged at 1500 g for 10 min. After washing three times, the final nuclear pellet was suspended as the nuclear fraction. The cytoplasmic and nuclear fractions in SDS loading buffer were separated by SDS-PAGE. Histone is a nuclear protein marker, and tubulin is a cytoplasmic protein marker. Anti-histone (Sigma-Aldrich, H0164, 1:2000 dilution), anti-tubulin (Sigma-Aldrich, T8203, 1:2000 dilution), anti-GFP (Abcam, ab13970, 1:2000 dilution), anti-phyA (1:1000 dilution),[46] and anti-phyB (1:1000 dilution)[33] antibodies were used for immunoblotting. For quantification, the relative protein levels in the nucleus were calculated as the protein levels in Nuc fractions divided by the total protein levels (Nuc proteins + Cyto proteins).

Immunoblot assays

Seedlings were harvested and ground to a fine powder in liquid nitrogen under dim green light in the dark room. The powder was homogenized in plant protein extraction buffer (50 mM Tris-HCl, pH=7.5, 150 mM NaCl, 1 mM EDTA, 0.25% Triton X-100, 1 mM PMSF), and the protein supernatant was collected by centrifugation. The protein supernatant in SDS loading buffer was separated by SDS-PAGE. Anti-PIF3 (1:1000 dilution),[92] anti-PIF1 (1:1000 dilution), anti-HSP (Thermo Fisher, MA1-10372, 1:3000 dilution), anti-GFP (Abcam, ab13970, 1:2000 dilution), anti-Myc (Sigma-Aldrich, M4439, 1:2000 dilution), anti-Actin (Sigma-Aldrich, A0480, 1:2000 dilution), and anti-RPN6 (Abmart, X-Q9LP45-N, 1:1000 dilution) antibodies were used for immunoblotting. A PIF1 antibody was generated against full-length PIF1 protein antigen in rabbit. For quantification, the relative protein levels were calculated by dividing with the mean of the protein levels detected in WT etiolated seedlings (D to R, 0 min), which was set to 100%.

RNA extraction and RT–qPCR

Total RNA was extracted and purified by using a Spectrum Plant Total RNA Kit (Sigma-Aldrich). RNA quality control was performed by gel electrophoresis and spectrophotometric analysis. Two micrograms of RNA were used for the synthesis of cDNA with ReverTra Ace qPCR RT Master Mix (Toyobo). SYBR Green Mix (Takara) was used for qPCR on ABI Fast 7500 real-time system. *PP2A* (*AT1G13320*) was used as reference genes for normalization.[92] Three technical replicates were averaged to calculate the value for each biological replicate, and three biological replicates were used for statistical analysis.

Firefly Luciferase Complementation Imaging (LCI) Assay

The full-length coding sequences of *CPK*s amplified from *Arabidopsis* cDNA by PCR were cloned into the pCAMBIA1300-LUC^c vector to generate CPK-LUC^c. The full-length coding sequences of phyB/D/E were cloned into the pCAMBIA1300-LUC^n vector to generate the phyB/D/E-LUC^n constructs. *Agrobacterium tumefaciens* carrying the indicated combinations of the CPK-LUC^c and phyB/D/E-LUC^n constructs was infiltrated into *Nicotiana benthamiana* leaves. After infiltration, tobacco plants were grown under white light for additional 3 days. A D-luciferin (Promega) solution was then infiltrated into the leaves, and luciferase activity was recorded using BERTHOLD TECHNOLOGIES LB985.

Protein expression and purification

The full-length coding sequences of *CPK6* and *CPK12* were cloned into the pMAL vector to generate the pMAL-CPK6/12 constructs. The MBP-CPK6/12 proteins were expressed in *E. coli* strain BL21 and purified using amylose resin (NEB). The coding sequence of the N-terminus of phyB (1-1830 bp) was cloned into the pET28a vector to generate the pET28a-phyBN construct. The pET28a-phyBN-80A/106A construct was generated by site-directed mutagenesis (Transgen, China). The His-phyBN and His-phyBN-80A/106A proteins were expressed in *E. coli* strain BL21 and purified by using Ni-NTA agarose (QIAGEN). The full-length coding sequence of phyB was cloned into the pFastBacHT B vector to generate the pFastBacHT B-phyB construct. The His-MBP-phyB protein was expressed in the High Five insect cell line and purified using HisTrap affinity chromatography (Sigma-Aldrich) as previously reported.[67]

Coimmunoprecipitation (Co-IP) Assays

Three-day-old etiolated seedlings were maintained in the dark or irradiated with red light for 0.5 h. Under dim green light in the dark room, the harvested seedlings were ground to a fine powder in liquid nitrogen and homogenized in lysis buffer (50 mM Tris-HCl, pH=7.5, 150 mM NaCl, 1 mM EDTA, 10% glycerol, 0.1% Tween 20, 1 mM PMSF and a Roche protease inhibitor cocktail). The supernatant was collected by cold centrifugation twice at 14000 rpm for 5 min. For semi in vitro Co-IP, purified recombinant MBP-CPK6 or MBP-CPK12 proteins were added and incubated by gentle rotation at 4 °C for 1 h. GFP-Trap agarose (Chromotek) or EZview Red c-Myc-Agarose (Sigma-Aldrich) were used for immunoprecipitation. Anti-MBP (NEB, E8032S, 1:2000 dilution), anti-Actin (Sigma-Aldrich, A0480, 1:2000 dilution), anti-RPN6 (Abmart, X-Q9LP45-N, 1:1000 dilution), anti-Myc (Sigma-Aldrich, M4439, 1:2000 dilution), anti-phyB (1:1000 dilution),[33] and anti-GFP (Abcam, ab13970, 1:2000 dilution) antibodies were used for immunoblotting.

For Co-IP in HEK293T cells, the indicated coding sequences were cloned into the pcDNA3.1 vector, and the recombinant proteins were expressed and extracted from HEK293T cells. Protein extracts containing phyB-2A-YFP were incubated with phycocyanobilin (PCB) on ice under 0.5 h of far-red or red light exposure to reconstitute the Pr or Pfr conformer, respectively. Equal amounts of protein extracts, as indicated, were incubated in binding buffer (20 mM Tris-HCl, pH=7.5, 150 mM NaCl, 1 mM EDTA) at 4 °C for 1 h with gentle rotation. GFP-Trap agarose (Chromotek) was used for precipitation and was then washed three times with washing buffer (50 mM Tris-HCl, 1 mM EDTA, 0.1% Triton X-100, and 10% glycerol). Anti-GFP (Abcam, ab13970, 1:2000 dilution), anti-HA (Cell Signaling Technology; C29F4, 1:1000 dilution), and anti-Myc (Sigma–Aldrich, M4439, 1:2000 dilution) antibodies were used for immunoblotting. For quantification, the relative co-IP protein levels were calculated by dividing with the mean of the most abundant co-IP protein levels detected, which was set to 100%.

In vitro Pull-down assays

Recombinant purified His-MBP-phyB proteins were incubated with phycocyanobilin (PCB) on ice under 0.5 h of far-red or red light exposure to reconstitute the Pr or Pfr conformer, respectively, as reported previously.[67,93] Equal amounts of the Pr or Pfr conformers of the His-MBP-phyB and MBP-CPK6/12 proteins were incubated in binding buffer (20 mM Tris-HCl, pH=7.5, 150 mM NaCl) in the presence of 0.5 mM $CaCl_2$ or 1 mM EGTA as indicated at 4 °C for 1 h with gentle rotation. Ni-NTA agarose (QIAGEN) was used for pull-down and was then washed three times with washing buffer (50 mM Tris-HCl, 1 mM EDTA, 0.1% Triton X-100, and 10% glycerol). An anti-MBP (NEB, E8032S, 1:2000 dilution) antibody was used for immunoblotting. For quantification, the relative bait protein levels were calculated by dividing with the mean of the most abundant bait protein levels detected, which was set to 100%.

In vitro phosphorylation assays

For phosphorylation analysis, 1 μg of substrate and 0.3 μg of kinase proteins in kinase buffer (150 mM Tris-HCl, pH=7.5, 200 mM NaCl, 10 mM $MgCl_2$, 20 μM ATP and 2 mM 6-Fu-ATPγS) supplemented with 0.5 mM $CaCl_2$ or 1 mM EGTA, as indicated, were incubated at 30 °C for 0.5 h.[38,94] Then, 2.5 mM PNBM (Abcam) was added, and the mixture was incubated at room temperature for 2 h. SDS loading buffer was added to stop the reactions. Phosphorylation was analyzed by immunoblotting with thiophosphate ester rabbit monoclonal antibody (Epitomics, #2686-1, 1:2000 dilution). Coomassie staining was used as a loading control. For quantification, the relative phosphorylated protein levels were calculated by dividing with the mean of the most abundant phosphorylated protein levels detected, which was set to 100%.

Immunoprecipitation Mass Spectrometry (IP-MS) Analyses

Sample preparation and digestion

Three-day old etiolated PBG seedlings were maintained in darkness or exposed to red light for 0.5 h. One gram of seedling materials was harvested and ground to a fine powder in liquid nitrogen under dim green light in the dark room. Total proteins were extracted in cold lysis buffer (50 mM Tris-HCl, pH=7.5, 150 mM NaCl, 1 mM EDTA, 10% glycerol, 0.1% Tween, 1 mM PMSF, 1× Roche protease inhibitor cocktail, and 1× Roche phosphatase inhibitor cocktail). The homogenate was centrifuged and filtered through microcloth. GFP-Trap agarose beads (Chromotek) were used for immunoprecipitation. The eluted proteins were separated by SDS-PAGE with Coomassie Blue Staining, and the phyB-GFP protein bands in the gels were excised. After dithiothreitol (DTT) reduction and iodoacetamide (IAA) alkylation, the proteins were digested with porcine trypsin (sequencing grade modified; PierceTM) and subjected to MS analyses.[95]

Easy-nLC Conditions

Using an Easy-nLC 1200 system (Thermo Fisher Scientific), samples were loaded at a speed of 280 nL/min onto a trap column (C18, Acclaim PepMap TM 100 75 μm x 2 cm nanoViper Thermo) and eluted across an analytical resolving column (C18, Acclaim PepMap TM 75 μm x 15 cm nanoViper RSLC Thermo) with a 75 min gradient. Buffer A consisted of 0.1% (v/v) formic acid in H_2O and Buffer B consisted of 0.1% (v/v) formic acid in 80% acetonitrile. The gradient was set as follows: 4%–8% B in 7 min; 8%–25% B in 68 min; 25%–35% B in 20 min; 35%–55% B in 20 min; 55%–90% B in 3 min; 90% B in 2 min.

Mass spectrometry conditions

Data-dependent tandem mass spectrometry (MS/MS) analysis was performed with a Thermo Orbitrap Fusion Lumos (Thermo Fisher Scientific) using a nano-electrospray ion source with an electrospray voltage of 2.2 kV. The MS full scan was performed using an Orbitrap Mass Analyzer (300-1500 m/z) with a resolution of 120,000 @ m/z 200, AGC target 5e5, and a maximum injection time of 50 ms, followed by MS/MS scans generated by HCD fragmentation at a resolution of 30,000 @ m/z 200. AGC target 5e4 and maximum injection time mode was set dynamic. Isolation width was set at 1.6 m/z and the HCD collision energy was set at 30%. MS scan functions and nLC solvent gradients were controlled by the Xcalibur data system (Thermo Fisher Scientific).

MS Data processing

Full MS and tandem mass spectra were extracted from raw files, and the tandem mass spectra were searched against the Uniprot *Arabidopsis thaliana* (Mouse-ear cress) [3702]_UP000006548 database using Proteome Discoverer 2.2 software (Thermo Fisher Scientific). The processing workflow includes Sequest HT, Percolator, PhosphoRS and Precursor Ions Quantifier (Thermo Proteome Discoverer User Guide). Enzyme specificity was set as trypsin and the maximum of missed trypsin cleavage sites as 2. The precursor mass tolerance was set to 10 ppm, and the fragment ion mass tolerance was set to 0.02 Da. Carbamidomethylation (C) was considered as a fixed modification. Oxidation (M) and acetylation (protein N-term) were variable modifications. Serine, threonine and tyrosine were treated as dynamically modified by +79.9663 Da for phosphorylation. The false discovery rate (FDR) applied at the peptide and protein levels was 1%. The threshold of PTM site probability using PhosphoRS was set as 99%. Precursor abundance of the indicated site was determined by area at the MS1 level using Precursor Ions Quantifier. The abundance ratio at a given site was calculated as the ratio of the abundance of phosphorylated residues to the total residue abundance.[96,97]

Sequence alignment

Arabidopsis thaliana phytochrome A-E and CPK subgroup I protein sequences were downloaded from the NCBI website (phyA GI: 3482934, phyB GI: 15224231, phyC GI: 15239211, phyD GI: 15234859, phyE GI: 240255991, CPK1 GI: 1032281076, CPK2 GI: 1032290200, CPK4 GI: 1032283773, CPK5 GI: 1032286569, CPK6 GI: 30679935, CPK11 GI: 15219693, CPK12 GI: 15237791, CPK20 GI: 1032295269, CPK25 GI: 1032293588, CPK26 GI: 332661500). The MAFFT website (https://mafft.cbrc.jp/alignment/server/) was used for the alignment of phytochrome A-E. MEGA software was used for CPK subgroup I sequence alignment and inferring the phylogenetic tree.

QUANTIFICATION AND STATISTICAL ANALYSIS

Cotyledon area and hypocotyl length were measured using ImageJ software (https://imagej.nih.gov/ij/). Observations of more than 10 seedlings were recorded for each sample. Immunoblot band intensity was quantified using ImageJ software. Student's *t* tests for two independent groups were performed using Microsoft Excel, with significant differences indicated as $^{*}P < 0.05$, $^{**}P < 0.01$, and $^{***}P < 0.001$. The sample size used for determining the mean and SD for each sample was presented in figure legends.

CellPress

Supplemental figures

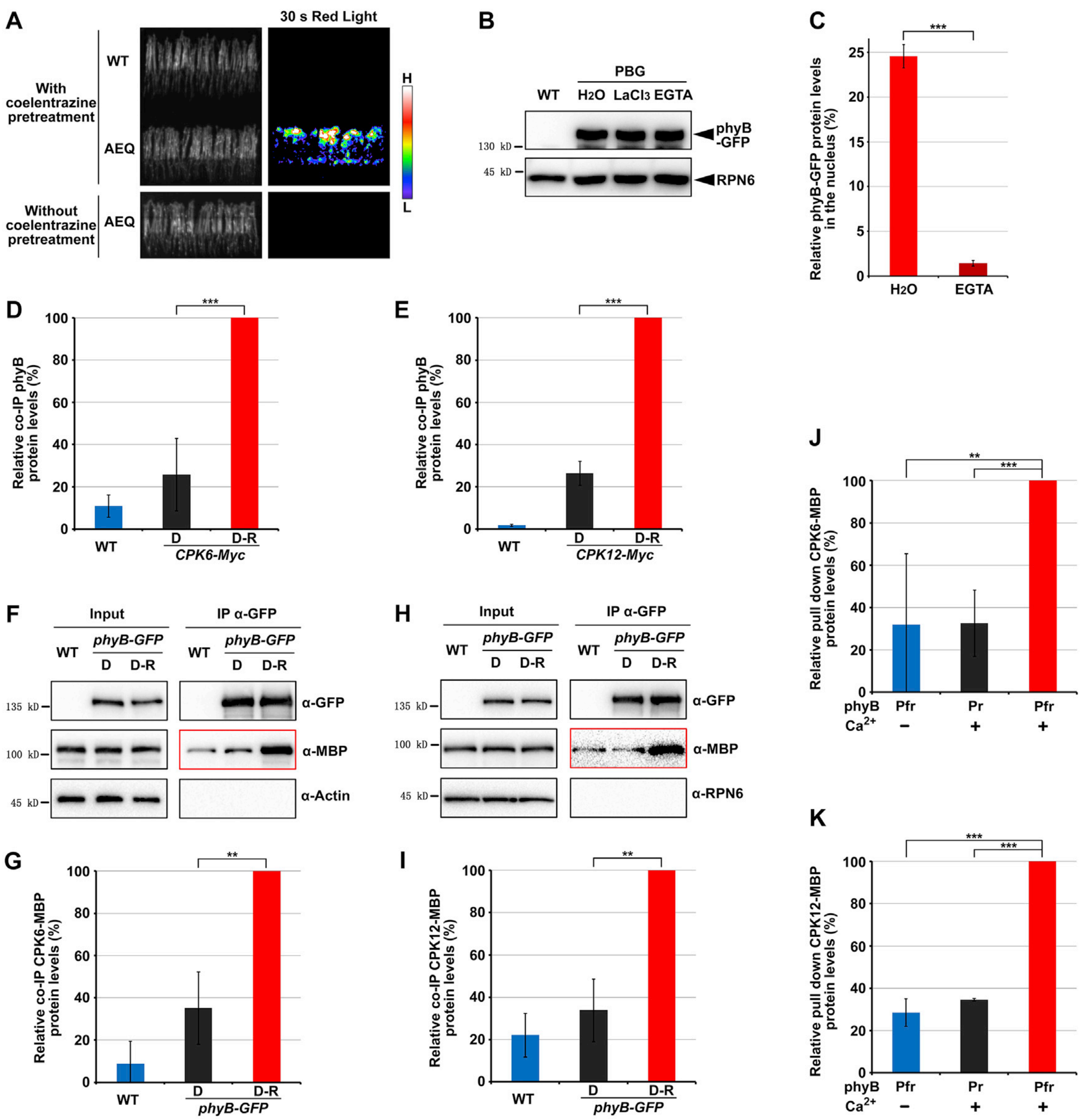

Figure S1. Ca^{2+} mediates phyB nuclear import and CPK6/12 interact with phyB, related to Figures 1 and 2

(A) Representative images of red-light-triggered-aequorin bioluminescence in *Arabidopsis* seedlings. WT and AEQ seedlings with coelentrazine pretreatment, and AEQ seedlings without coelentrazine pretreatment were imaged. Etiolated seedlings were irradiated with 30 s of red light, followed by imaging.

(B) phyB-GFP protein levels are not altered by the treatment of Ca^{2+} signaling inhibitors. PBG etiolated seedlings under H_2O, 5-mM $LaCl_3$ or 5-mM EGTA treatment were irradiated with red light.

(C) Quantification of the subcellular fractionation analysis of phyB-GFP proteins in Figure 1J. Mean ± SD, n = 3.

(D and E) Quantification of the coIP assays of phyB and CPK6/12 in Figures 2C and 2D. Mean ± SD, n = 3.

(F–I) Semi *in vivo* coIP assays showing the red-light-stimulated interaction between phyB and CPK6/12. PBG etiolated seedlings were either maintained in the dark (D) or irradiated with red light (D to R) for 0.5 h and were then subjected to extraction. Purified recombinant MBP-CPK6 (F and G) or MBP-CPK12 (H and I) protein was incubated with protein extracts. The representative immunoblot images (F and H) and quantification results (G and I) were shown. Mean ± SD, n = 3.

(J and K) Quantification of the *in vitro* pull-down assays of phyB and CPK6/12 in Figures 2E and 2F. Mean ± SD, n = 3.

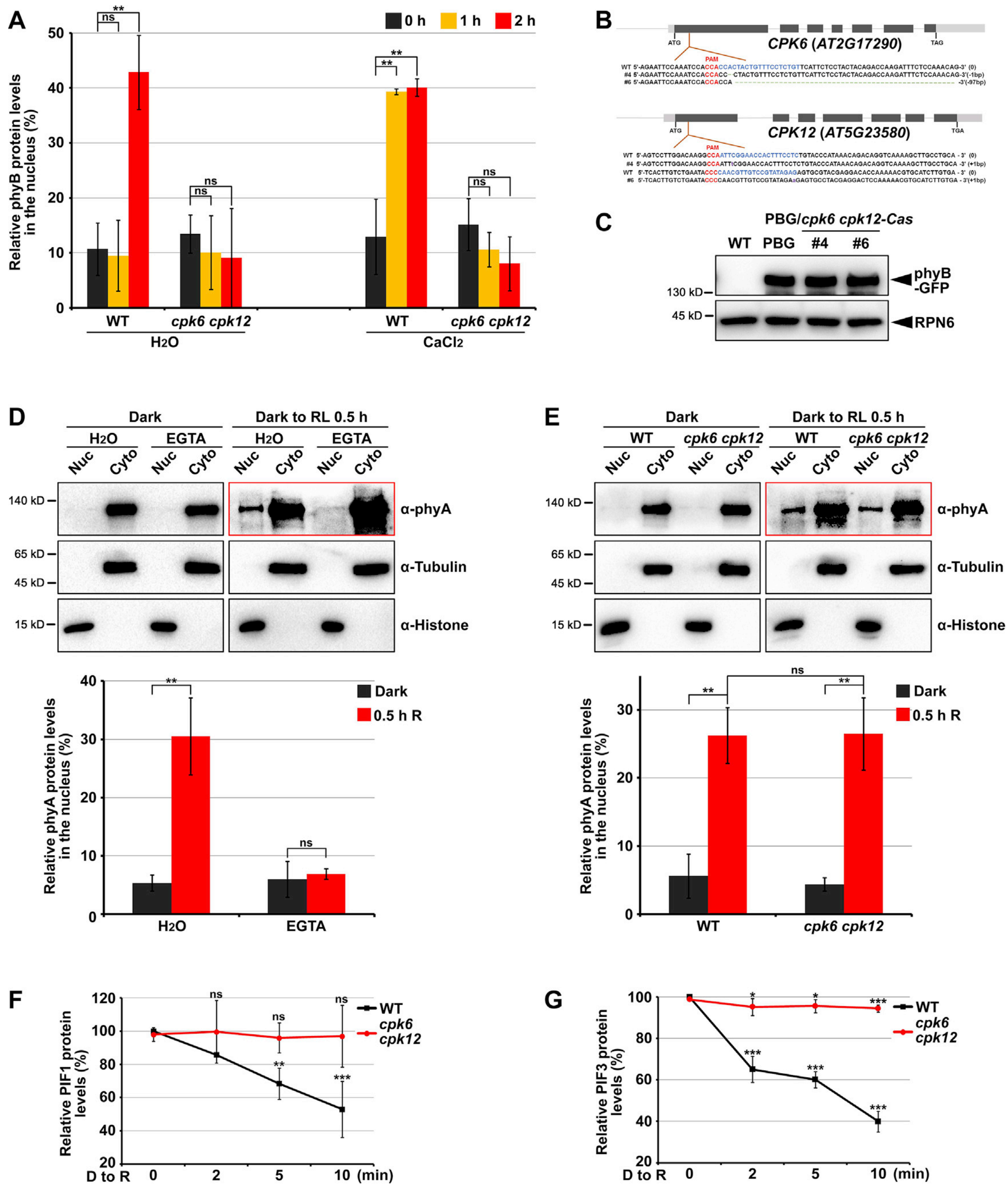

Figure S2. CPK6/12 are required for red-light-induced phyB but not phyA nuclear import to mediate subsequent PIF degradation, related to Figure 3

(A) Quantification of the subcellular fractionation analysis of phyB proteins in Figure 3A. Mean ± SD, n = 3.

(B) DNA sequence information of the *CPK6* and *CPK12* loci edited by the CRISPR-Cas9 system in the PBG background. #4 and #6 are two independent transgenic lines.

(C) Western blot results showing that phyB-GFP protein levels are not altered by the mutation of *CPK6/12*. Etiolated seedlings were irradiated with red light.

(D and E) Western blot results showing that CPK6/12 are not involved in red-light-induced nuclear import of phyA. Etiolated WT seedlings with H_2O or 5-mM EGTA treatment (D), or etiolated WT and *cpk6 cpk12* seedlings (E), were maintained in darkness or exposed to 10 μmol m^{-2} s^{-1} red light for 0.5 h. The representative immunoblot images (top) and quantification results (bottom) were shown. Mean ± SD, n = 3.

(F and G) Quantification of the light-induced PIF protein degradation in Figure 3C. Mean ± SD, n = 3.

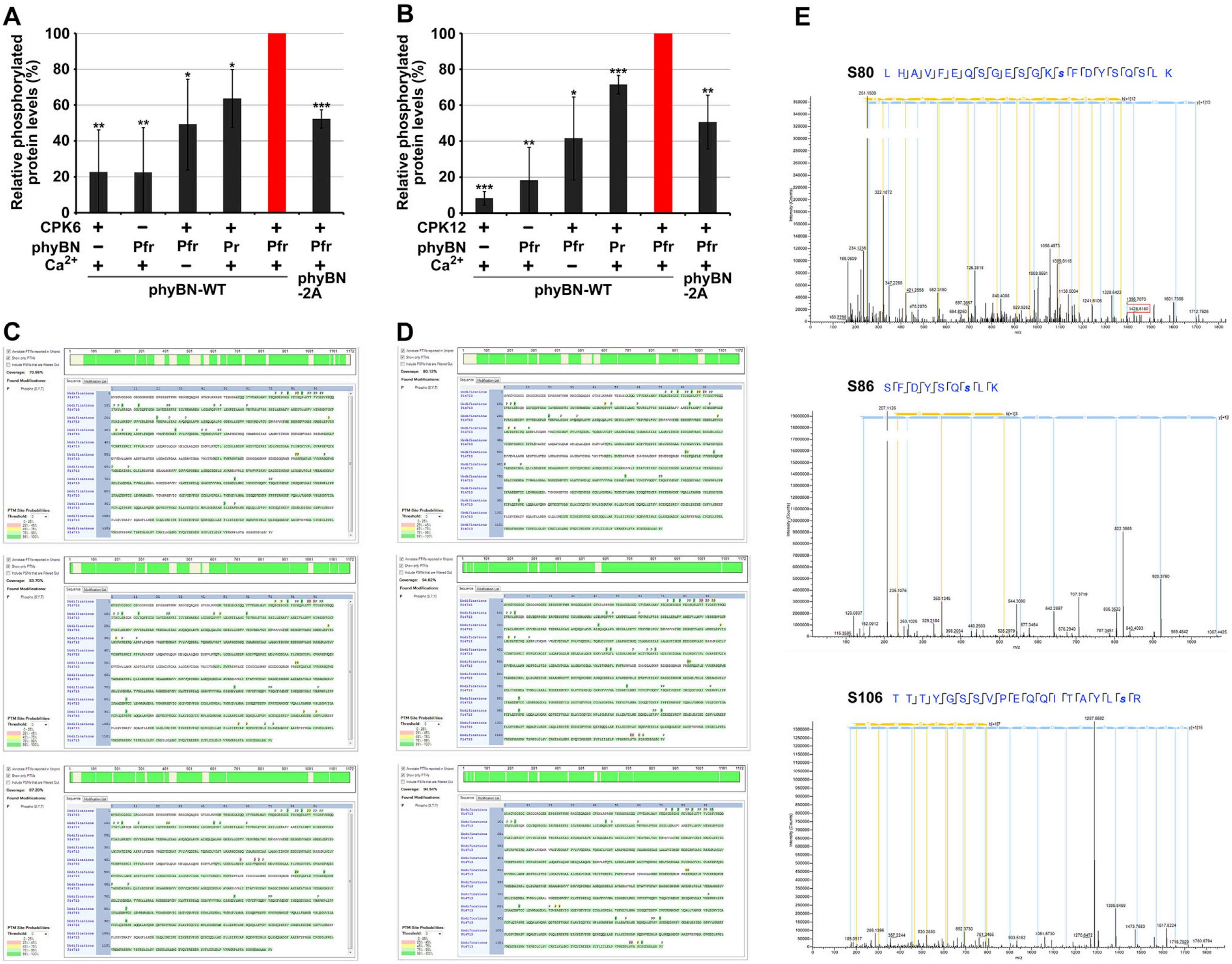

Figure S3. Mass spectrometric analyses of phyB phosphosites during dark-to-light transition, related to Figure 4

(A and B) Quantification of *in vitro* kinase assays of phyB by CPK6/12 in Figures 4A and 4B. Mean ± SD, n = 3.

(C and D) Mass spectrometric analyses of phyB phosphosites in three biological replicates. Etiolated PBG seedlings were maintained in darkness (C) or irradiated with red light for 0.5 h (D).

(E) Representative tandem mass spectrum of phosphopeptides showing that S80, S86, and S106 were phosphorylated *in vivo*.

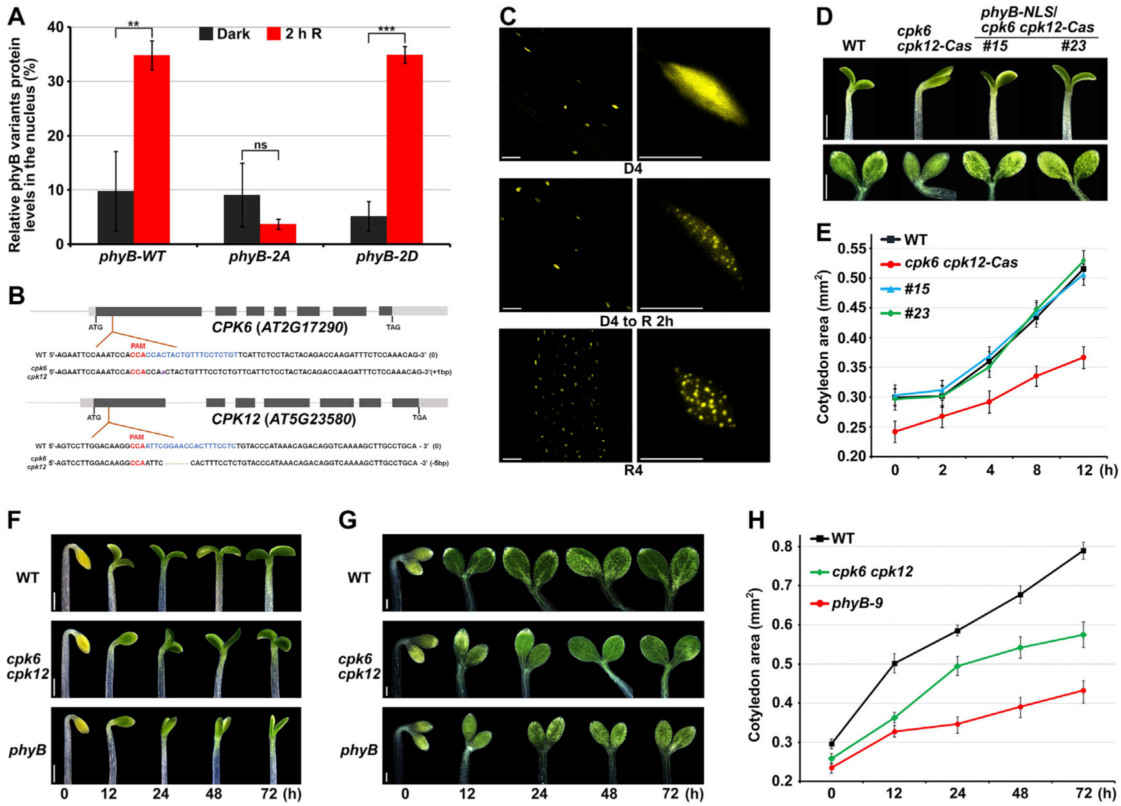

Figure S4. The de-etiolation defects of *cpk6 cpk12* mutant were fully restored by an NLS-fused phyB and were attenuated by prolonged red light irradiation, related to Figures 4 and 5

(A) Quantification of the subcellular fractionation analysis of the YFP-fused phyB variants in Figure 4E. Mean ± SD, n = 3.

(B) DNA sequence information of the *CPK6* and *CPK12* loci edited using the CRISPR-Cas9 system in *35S:phyB-NLS/cpk6 cpk12-Cas* (*phyB-NLS/cpk6 cpk12-Cas*) plants.

(C) Subcellular fluorescence observations of the NLS-fused phyB-YFP proteins in seedlings. 4-day-old *phyB-NLS/cpk6 cpk12-Cas* seedlings were grown in darkness without (D4) or with 2 h of red light exposure (D4 to R 2 h) or were grown under continuous red light exposure (R4). Scale bars, 50 μm (left) and 10 μm (right).

(D–H) Representative cotyledon opening (D, top; F) and expansion phenotypes (D, bottom; G) of etiolated seedlings subjected to 10 μmol m^{-2} s^{-1} red light irradiation for 12 h (D and E), or for the indicated periods (F and G), were shown. Scale bars: 0.5 mm in (D) and (F) and 0.2 mm in (G). The cotyledon areas in a red light irradiation time course experiment were quantified (E and H). Mean ± SD, n ≥ 10.

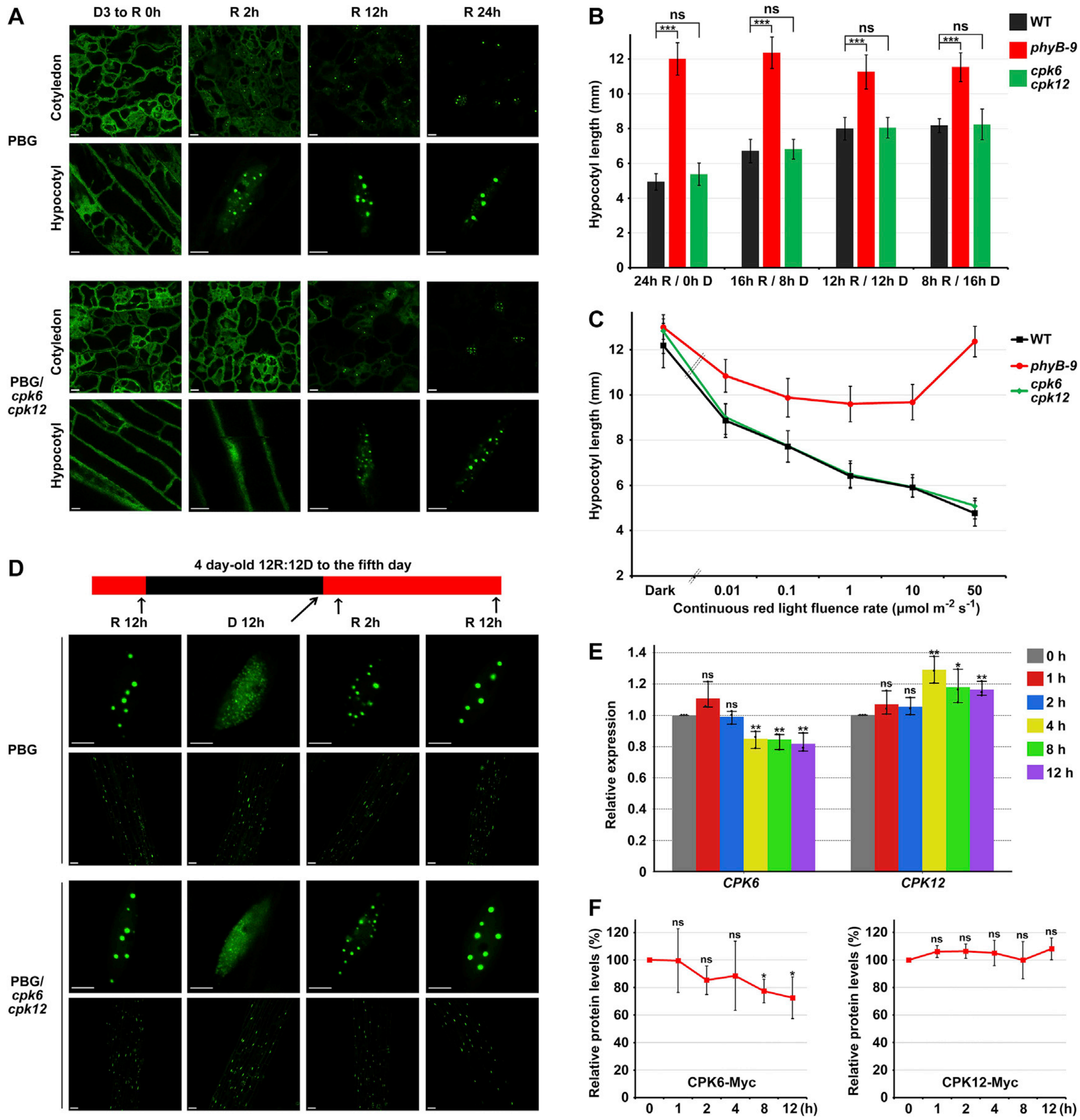

Figure S5. CPK6/12 regulate phyB nuclear import to promote de-etiolation transition specifically in etiolated seedlings upon initial light exposure, related to Figure 5

(A) Subcellular fluorescence observations of phyB-GFP in the hypocotyl and cotyledon cells in etiolated seedlings with red light irradiation. Etiolated seedlings were irradiated with red light for the indicated periods. Scale bars, 5 μm.

(B and C) The hypocotyl elongation of seedlings grown in various day-night conditions (B), or under continuous red light of different light fluence rates (C) for 5 days. Mean ± SD, n ≥ 10.

(D) Subcellular fluorescence observations of phyB-GFP in seedlings grown under day-night (12 h/12 h) condition and phyB-GFP signals were observed at the indicated time points. Scale bars, 5 μm (top) and 50 μm (bottom).

(E) RT-qPCR results showing the gene expression levels of *CPK6* and *CPK12* during dark-to-light transition. Etiolated seedlings were exposed to red light for the indicated periods. Mean ± SD, n = 3.

(F) Quantification of immunoblot analysis of CPK 6 and CPK12 protein levels during dark-to-light process. *35S:CPK6-Myc* (left) or *35S:CPK12-Myc* (right) etiolated seedlings were exposed to red light for the indicated periods. Mean ± SD, n = 3.

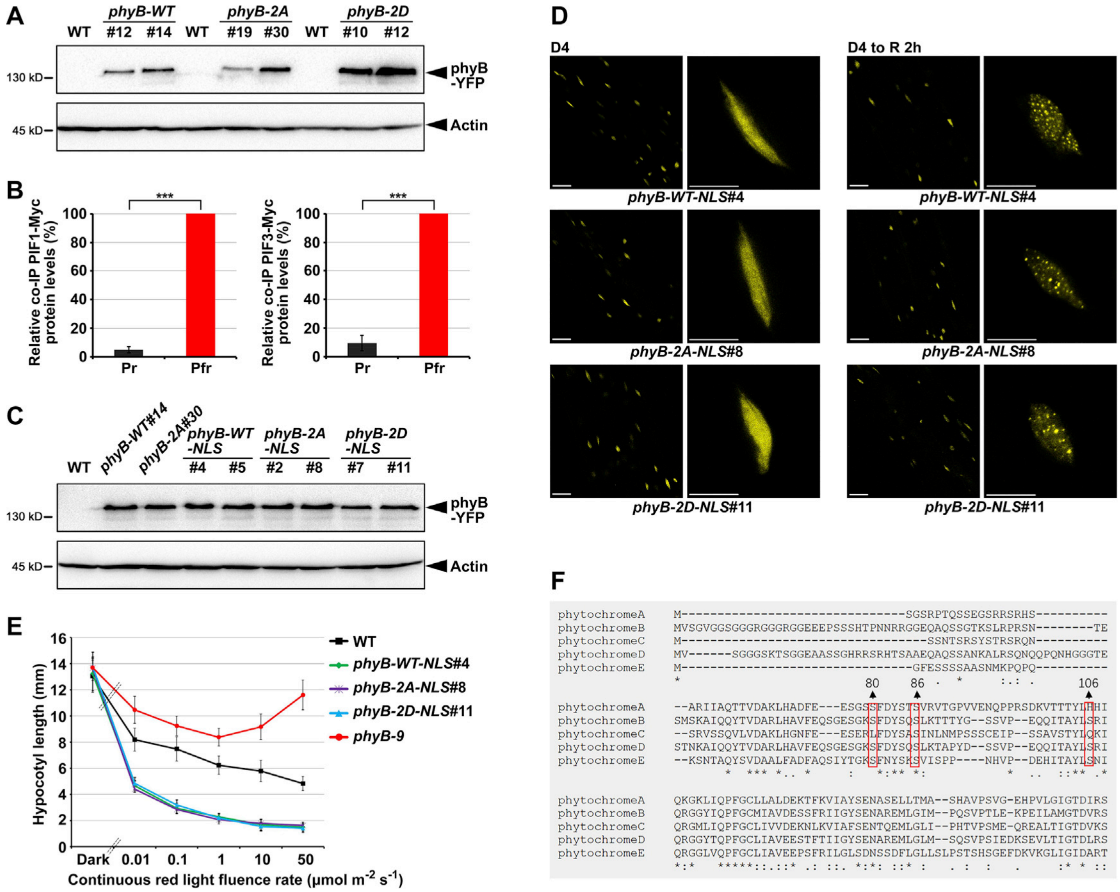

Figure S6. S80/S106 phosphorylation does not affect phyB activity, related to Figures 5 and 6

(A and C) Western blot results indicating protein levels of various version phyB-YFPs in 5-day-old red-light-grown transgenic seedlings.

(B) Quantification of the coIP assays of phyB-2A and PIFs in Figure 6A. Mean ± SD, n = 3.

(D) Subcellular fluorescence observations showing that NLS-fused phyB-YFP variants are constitutively localized in the nucleus and exhibit normal light-induced photobody formation. 4-day-old, etiolated seedlings were maintained in the dark (D4) or transferred to red light exposure (D4 to R 2 h) for 2 h. Scale bars, 50 μm (left) and 10 μm (right).

(E) Fluence rate response curves for hypocotyl lengths of transgenic seedlings expressing NLS-fused phyB variants. Seedlings were grown in darkness or under continuous red light of different light fluence rates for 5 days. Mean ± SD, n ≥ 10.

(F) Alignment of *Arabidopsis* phytochrome A-E amino acids. The amino acid sequences of the five phytochrome proteins were aligned by using MAFFT (V7.452). The residues aligned to phyB S80, S86, and S106 are indicated in the red box.

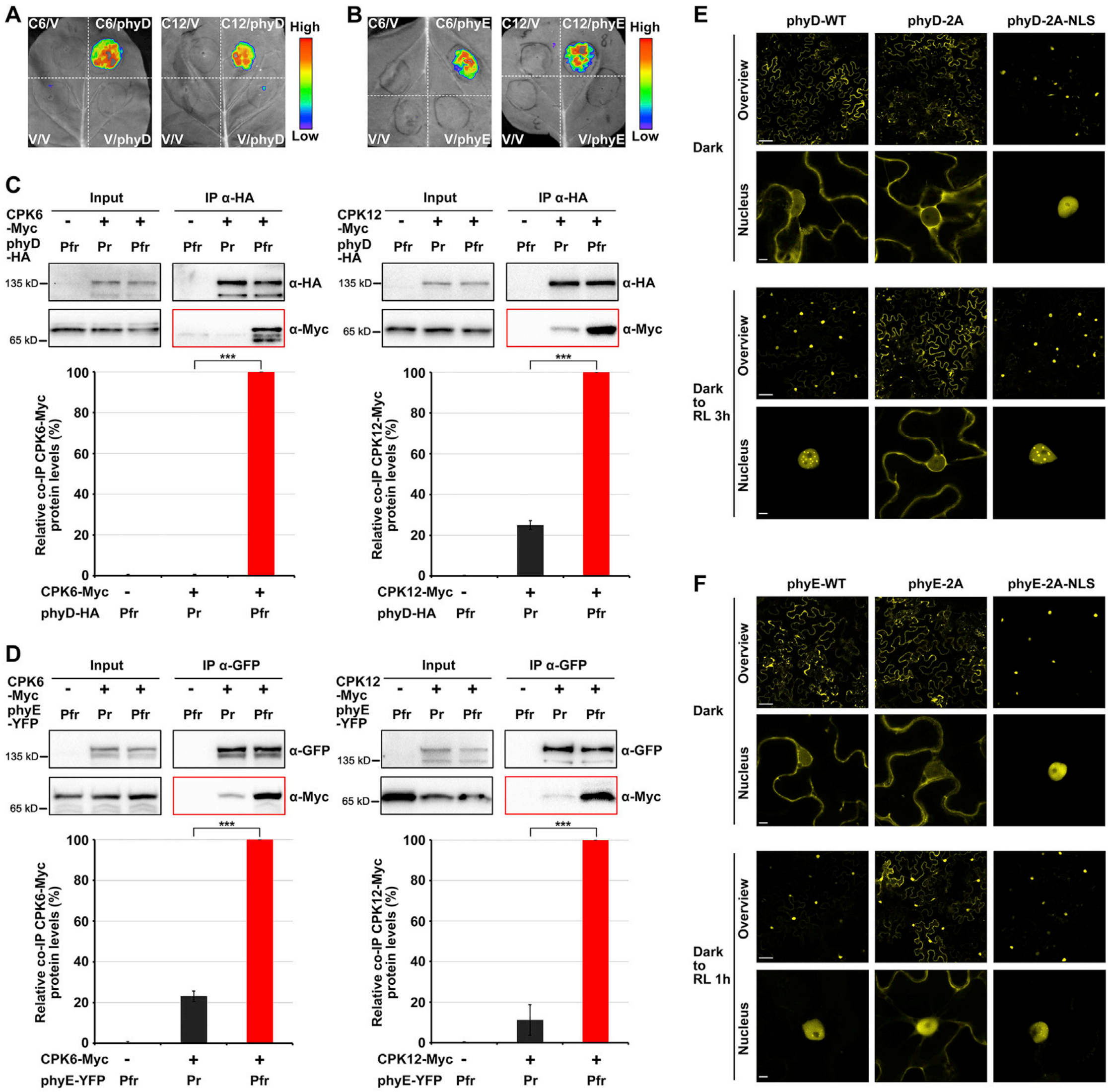

Figure S7. CPK6/12 phosphorylation-determined nuclear translocation could be conserved in the phyB/D/E lineage, related to Figure 7

(A and B) LCI assay showing the protein-protein interactions of phyD and phyE with CPK6/12 in tobacco leaves. Full-length phyD (A) or phyE (B) was fused in frame with the split N terminus of luciferase (LUC^n). Full-length CPK6 (C6) or CPK12 (C12) was fused in frame with the split C terminus of luciferase (LUC^c). V, empty vector.

(C and D) CoIP assays showing the light-dependent interactions of phyD/E and CPK6/12. The representative immunoblot images (top) and quantification results (bottom) were shown. Mean ± SD, n = 3.

(E and F) Subcellular fluorescence observations of YFP-fused phyD and phyE variants in tobacco leaves. The dark-adapted tobacco plants were maintained in darkness (dark) or irradiated by 3 h of 10 μmol m^{-2} s^{-1} red light for phyD or 1 h of 1 μmol m^{-2} s^{-1} red light for phyE (dark to RL). Scale bars, 50 μm (top) and 5 μm (bottom).